Atmos. Meas. Tech., 11, 3737–3757, 2018 https://doi.org/10.5194/amt-11-3737-2018 © Author(s) 2018. This work is distributed under the Creative Commons Attribution 4.0 License.





The IAGOS NO_x instrument – design, operation and first results from deployment aboard passenger aircraft

Florian Berkes¹, Norbert Houben¹, Ulrich Bundke¹, Harald Franke², Hans-Werner Pätz¹, Franz Rohrer¹, Andreas Wahner¹, and Andreas Petzold¹

¹Forschungszentrum Jülich, IEK-8, Jülich, Germany

Correspondence: Florian Berkes (f.berkes@fz-juelich.de) and Andreas Petzold (a.petzold@fz-juelich.de)

Received: 30 November 2017 – Discussion started: 22 December 2017 Revised: 18 April 2018 – Accepted: 30 May 2018 – Published: 27 June 2018

Abstract. We describe the nitrogen oxide instrument designed for the autonomous operation on board passenger aircraft in the framework of the European Research Infrastructure IAGOS (In-service Aircraft for a Global Observing System). We demonstrate the performance of the instrument using data from two deployment periods aboard an A340-300 aircraft of Deutsche Lufthansa. The well-established chemiluminescence detection method is used to measure nitrogen monoxide (NO) and nitrogen oxides (NO_x). NO_x is measured using a photolytic converter, and nitrogen dioxide (NO_2) is determined from the difference between NO_x and NO. This technique allows measuring at high time resolution (4s) and high precision in the low ppt range (NO: $2\sigma = 24$ pptv; NO_x: $2\sigma = 35$ pptv) over different ambient temperature and ambient pressure altitude ranges (from surface pressure down to 190 hPa). The IAGOS NO_x instrument is characterized for (1) calibration stability and total uncertainty, (2) humidity and chemical interferences (e.g., ozone; nitrous acid, HONO; peroxyacetyl nitrate, PAN) and (3) inter-instrumental precision. We demonstrate that the IA-GOS NO_x instrument is a robust, fully automated, and longterm stable instrument suitable for unattended operation on airborne platforms, which provides useful measurements for future air quality studies and emission estimates.

1 Introduction

Monitoring of NO_x (= $NO + NO_2$) in the atmosphere is important for estimating the amount of natural and anthropogenic NO_x emissions, for assessing air quality (e.g., for-

mation of ozone and secondary aerosols) and concerning the climate impact of ozone. Ozone is a strong greenhouse gas and contributes to global radiative forcing (IPCC, 2007; Fahey and Lee, 2016) and to changes in global dynamics (Fueglistaler et al., 2014). Close to ground ozone has an impact on human health (Skalska et al., 2010) and causes ecosystem damage (Ainsworth et al., 2012); NO₂ by itself poses a public health risk as well. Therefore knowledge of the spatial distribution of NO_x is important to identify the sources, sinks and its partitioning between NO and NO_2 in the atmosphere (Monks et al., 2009).

It is known that the global NO_x budget contains contributions from natural sources of NO_x – like lightning (LNO_x) , biomass burning and soil emissions – as well as from anthropogenic sources, such as power generation, road transportation and aviation. Current knowledge of the global distribution of NO_x and its emission estimates is based mostly on surface monitoring stations (Aerosols, Clouds and Trace gases Research Infrastructure, ACTRIS; https://www.actris.eu, last access: 29 November 2017), satellite measurements (Fishman et al., 2008; de Laat et al., 2014; Duncan et al., 2016) and model simulations (Ehhalt et al., 1992; Emmons et al., 1997).

The satellite retrievals provide tropospheric NO₂ columns, which are defined as the vertically integrated NO₂ number density between the surface and the tropopause. Satellite data users are provided with averaging kernels, which give the relationship between the true vertical profile and what is actually measured (Eskes and Boersma, 2003). The new experiment TROPOMI (TROPOspheric Monitoring Instrument) on Sentinel-5P provides global coverage with a spatial res-

²enviscope GmbH, Frankfurt, Germany

olution of $7 \times 7 \text{ km}^2$. The instrument covers spectral bands at different wavelengths, including bands in the ultraviolet (UV) spectrum up to the shortwave infrared (SWIR) spectrum. These bands are selected to measure the most relevant species in the troposphere and to improve cloud correction retrievals (Veefkind et al., 2012).

In the upper troposphere and lowermost stratosphere (UTLS), emissions from cruising passenger aircraft form another important source of NO_x , with its source strength being determined from civil aviation traffic data and specific emission factors (Emmons et al., 1997; Rohrer et al., 1997; Schumann and Huntrieser, 2007; Ziereis et al., 2000; Gressent et al., 2016). Aircraft campaigns conducted in the past have made considerable progress in improving the estimate of the emissions of aviation (Schumann and Huntrieser, 2007; Lee et al., 2010; Wasiuk et al., 2016); in improving the estimate of LNO_x emissions over different regions, summarized by Gressent et al. (2016); and in increasing knowledge of deep convectively lifted pollutants and their burden to ozone chemistry (Huntrieser et al., 2016). However, these and other research aircraft campaigns lack the statistical robustness of comprehensive seasonal and geographical coverage of the UTLS region.

Despite the progress made on modeling aviation's impacts on tropospheric chemistry, there remains a significant spread in model results (Lee et al., 2010). Parameterization of natural NO_x emissions by lightning still has large uncertainty in global chemical transport models (e.g., Gressent et al., 2016). Brunner et al. (2005) and Prather et al. (2017) concluded that a better description of emissions, chemistry and sinks of NO_x (and other key species) is needed to improve chemistry in the UTLS region in global chemistry models.

Using passenger aircraft equipped with instruments for measuring NO_x as a measurement platform can help to link satellite and surface measurements, and to fill the UTLS gap where otherwise no regular in situ observations are possible. Global-scale NO_x observations in the upper troposphere are particularly important regarding long-range transport of pollutants and its burden to regional air quality (Petzold et al., 2015). Since 1994, the European Research Infrastructure IAGOS (In-service Aircraft for a Global Observing System, https://www.iagos.org/) has provided in situ observations of essential climate variables (temperature, water vapor, and ozone, and other species later on) on a global scale from the surface up to 13 km altitude (Petzold et al., 2015). IAGOS builds on the former EU framework projects MOZAIC (Measurement of Ozone and Water Vapour by Airbus In-service Aircraft; Marenco et al., 1998) and CARIBIC (Civil Aircraft for the Regular Investigation of the atmosphere Based on an Instrument Container; Brenninkmeijer et al., 2007). Between 2001 and 2005, total odd nitrogen ($NO_v = NO$ and its atmospheric oxidation products, such as nitrogen dioxide, NO₂; nitric acid, HNO₃; and peroxyacetyl nitrate, PAN) was measured on MOZAIC (Volz-Thomas et al., 2005; Pätz et al.,

2006), and since 2005 it has been measured on CARIBIC (Stratmann et al., 2016).

Based on the IAGOS data sets, Thomas et al. (2015) and Stratmann et al. (2016) presented the geographical distribution and seasonal variation of NO_v at cruising altitude over the different periods, whereas Gressent et al. (2014) showed that the majority of large-scale plumes of NO_v are related to long-range transport and only a minor fraction to LNO_x in the UTLS over the North Atlantic region. On the other hand, Brunner et al. (2001) demonstrated from a 1-year climatology of NO_x in the UTLS region, from the Swiss NOXAR (measurements of Nitrogen OXides and ozone along Air Routes) program the importance of and need for statistical robustness of comprehensive seasonal and geographical coverage of NO_x measurements. However, NO₂ was mostly not trustable from these measurements (contamination, instrument failure) at that time, and therefore NO₂ is based on calculations of the photochemical state. This accounts also for the CARIBIC platform where NO₂ is only available from daytime calculation from the photochemical state (Stratmann et al., 2016).

Given its important role in atmospheric chemistry and the resulting needs for global-scale regular measurements, it was decided to develop a NO_x-specific instrument for the operation in the framework of IAGOS, which we describe here. The most common measurement technologies for NO_x are based on the chemiluminescence detection (CLD) for the indirect measurement of NO (Clough and Thrush, 1967; Ridley and Howlett, 1974; Drummond et al., 1985; Fahey et al., 1985). CLD instruments have often been coupled to a photolytic or catalytic converter to measure NO₂ and NO_x by using a xenon lamp, blue-light converter or catalytic conversion of NO₂ into NO, prior to the CLD unit (Fehsenfeld et al., 1990; Ryerson et al., 2000; Nakamura et al., 2003; Pollack et al., 2010; Villena et al., 2012; Reed et al., 2016). NO2 measurements at low-NO $_x$ conditions (below 0.1 ppbv) are close to the limit of detection (Yang et al., 2004), and depending on the installed converter each instrument might show interferences with other nitrogen-oxide-containing species (e.g., Reed et al., 2016).

To minimize these chemically driven interferences, recent instruments have been developed from optical techniques to measure NO₂ by light absorption with cavity ringdown spectroscopy (CRDS; Fuchs et al., 2010; Wagner et al., 2011), cavity-attenuated phase shift (CAPS; Kebabian et al., 2008), laser-induced fluorescence (LIF; Thornton et al., 2000) and differential optical absorption spectroscopy (DOAS; Platt and Stutz, 2008). However, most of these instruments have a detection limit above 0.1 ppbv, or the instrument size and weight is too large to be used for routine aircraft observations (Fuchs et al., 2010; Brent et al., 2015).

In the following, we present the technique, design, calibration and quality assurance (QA) of the IAGOS NO_x instrument in Sect. 2, followed by details about the data processing (Sect. 3) and the instrument performance (Sect. 4). First ap-

plications of the new instrument aboard an A340-300 aircraft of Deutsche Lufthansa are given in Sect. 5.

2 IAGOS NO_x instrument Package 2b measurement system and calibration

The design of the IAGOS NO_x instrument Package 2b (P2b) is based on the former MOZAIC NO_v instrument described by Volz-Thomas et al. (2005) and Pätz et al. (2006), using the CLD method for NO with a photolytic converter to convert NO₂ into NO. When using passenger aircraft as platform, many conflicting needs have to be fulfilled: the instrument has to be fully automated, small and lightweight, with limited power consumption, and fulfill high safety standards (mechanical stability, electromagnetic interference and flammability specifications). Furthermore, easy access, simple installation and long deployment periods of up to 6 months have to be guaranteed, while it should measure at NO_x mixing ratios as low as 0.1 ppbv and below with the highest possible temporal resolution, accuracy and reliability over the widely varying conditions of external temperature (-70 to +40 °C) and pressure (190 to 1000 hPa) in an unattended

The IAGOS NO_x instrument is installed on an IAGOS-CORE mounting rack, which is located in the avionics bay of an A340-300 aircraft (Fig. 1). The mounting rack provides all electrical, pneumatic and safety provisions required for operation. For data transfer the instrument is connected via Ethernet to IAGOS Package 1 (P1), which handles the data transfer for all IAGOS instruments on board (Nédélec et al., 2015). P1 is installed on every IAGOS-CORE aircraft and provides measurements of ozone, carbon monoxide, temperature, water vapor and a number of cloud particles (hydrometeors). It also records relevant parameters like position, static pressure, velocity, etc. from the avionics system of the aircraft (Petzold et al., 2015). The uncertainty of ozone is given with 2 ppbv \pm 2 %, and the uncertainty of water vapor is 5 % over liquid water (Nédélec et al., 2015; Neis et al., 2015).

2.1 Instrument design

Figure 2 shows the schematic flow and position of the major components of the IAGOS NO_x instrument. The following sections present a detailed description of the detection method (Sect. 2.1.1); of the reaction cell and the photomultiplier (PMT) as the primary detector hosted in the NO detector (NOD) unit (Sect. 2.1.2); of the ozone generator (O3G); of the photolytic converter (Sect. 2.1.3); and of the inlet manifold (Sect. 2.1.5), residence time characterization (Sect. 2.1.6) and internal stability checks (Sect. 2.1.7) of the inlet, converter and calibration assembly (ICC). A description of the instrument operation is provided in Sect. 2.1.7. The NO detector sensitivity and the converter efficiency are determined in the laboratory (Sect. 2.2). Tables 1 and 2 pro-



Figure 1. Position of Package 1 and Package 2 installed aboard the Airbus A340-300. The inlet plate including the Rosemount housing is attached at the aircraft skin.

vide an overview of the instrument specification and the main instrument parameters.

2.1.1 The chemiluminescence detection method

The CLD method is a well-established technique to detect NO by reaction with excess ozone. NO_x is measured by converting NO_2 into NO. This converted NO_x is often called NO_c at this stage.

$$NO + O_3 \rightarrow NO_2 + O_2 \tag{R1}$$

$$NO + O_3 \rightarrow NO_2^* + O_2 \tag{R2}$$

$$NO_2^* \rightarrow NO_2 + hv \quad (\lambda > 600 \,\text{nm})$$
 (R3)

$$NO_2^* + M \rightarrow NO_2 + M \quad (M = N_2, O_2)$$
 (R4)

In measuring mode (MM) the sample air is mixed with ozone in the reaction cell where NO is oxidized by Reactions (R1) or (R2). The photons released in Reaction (R3) are detected by a photomultiplier tube (Hamamatsu R2228P or Electron Tubes Enterprises 9828A, depending on the individual instrument) which is operated in photon-counting mode. In zero mode (ZM), ozone is mixed with the sample air before the pre-chamber (a 30 to 50 cm long 1/8 in. outer diameter stainless-steel tube) in order to oxidize most of the NO before it reaches the reaction cell. The volume and thus the sample residence time of the pre-chamber are adjusted such that 97 to 99 % of the NO is oxidized before the sample air reaches the reaction cell. The photon count rate in zero mode includes the background signal of the photomultiplier (caused by photons originating from the thermal radiation) and additional interferences from other chemical reactions (Drummond et al., 1985). The count rate is quite stable, ex-

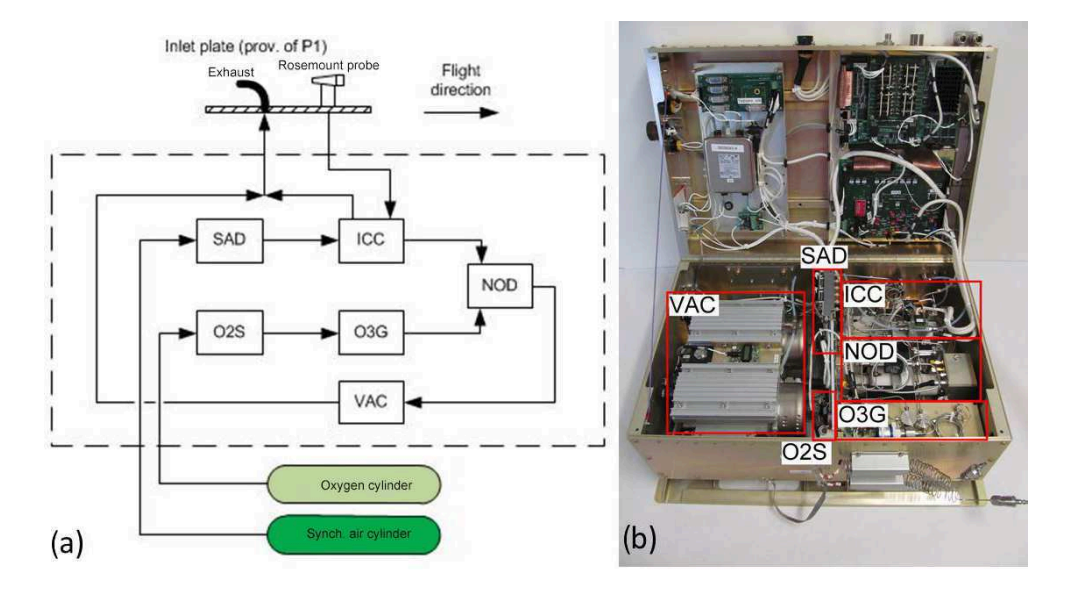


Figure 2. Schematic diagram of the IAGOS NO_x instrument (Revision 2, certification in progress) showing all connections and modules. A more detailed view is shown in the Supplement (Fig. S1). O2S and SAD: assembly with magnetic valves and capillaries for distribution of oxygen and synthetic air to different parts of the instrument. NOD: chemiluminescence detector. O3G: ozone generator. VAC: two membrane pumps for the gas flow of the system. ICC: internal calibration and converter unit, containing the manifold, photolytic converter, flow controller and permeation source. In Revision 1 only O_2 is used for the internal stability checks during flight, while in Revision 2 this is replaced by synthetic air. O_2 is then only used for the ozone generator.

Table 1. Overview of the main instrument components and their specification.

Part of instrument	Material/manufacturer	Geometrics. V: volume; L: length; OD: outside diameter	Pressure	Residence time
Inlet tube	FEP	L: 900 mm, OD: 1/8 in.	Ambient	< 0.05 s
Manifold	Stainless steel	V: 0.3 mL	Ambient	2.5 to 12 s
Photolytic converter	borosilicate glass	V: 25 mL	Ambient	
Pre-chamber	Stainless steel	L: 300 to 500 mm, OD: 1/8 in.	10 hPa	< 0.04 s
Reaction chamber	Gold-plated stainless steel	V: 28 mL	10 hPa	
Photomultiplier	Hamamatsu R2228P	_		
-	Electron Tubes Enterprises 9828A			

Table 2. IAGOS NO $_x$ instrument specification.

Quantity	Value
Sample flow rate	150 sccm
Inlet flow rate	1.5 SLM
Weight	29 kg
Dimensions $(L \times W \times H)$	$560 \times 400 \times 283 \mathrm{mm}$
Deployment period	Ca. 6 months
Time resolution of photon count rate	10 Hz

cept during takeoff, due to warming up (or cooling down) of different components in the instrument (e.g., ozone generator, PMT). The mixing ratio $(X, X \in \{NO, NO_2\})$ is determined from the difference of the photon count rates measured

in measuring mode and zero mode divided by the detector sensitivity (S_{NOD}) and the conversion efficiency (E_{PLC}) in the case of NO₂:

$$[X] = \frac{MM - ZM}{S_{\text{NOD}} \times E_{\text{PLC}}}.$$
 (1)

2.1.2 The detector and reaction cell

The chemiluminescence detector mounted in the NOD unit is similar to that described by Volz-Thomas et al. (2005). The PMT is cooled by four Peltier elements to temperatures below $-10\,^{\circ}\text{C}$ at an instrument temperature ($T_{\text{Instrument}}$) of $20\,^{\circ}\text{C}$. The reaction cell is separated from the PMT housing by a 1 mm thick window and a low-pass red-light filter. This setup provides thermal insulation and limits the light reaching the PMT to wavelengths below $600\,\text{nm}$. The space be-

tween the cell window and the low-pass filter, as well as the PMT housing, is purged with a small flow of O_2 or synthetic air $(0.2\,\mathrm{mL\,min^{-1}})$ to avoid condensation. The reaction cell is operated at a pressure of approximately 10 mbar. We learned from the MOZAIC NO_y instrument that the cell does not require power-consuming temperature control because of the relatively stable temperature in the avionics compartment. The temperature is measured, however, in order to allow for potentially necessary corrections of the sensitivity.

2.1.3 O₃ generator

The ozone is generated in an oxygen flow (approximately 20 sccm) through a ceramic discharge tube with a coaxial inner stainless-steel electrode of 3mm diameter, which is connected to a HV transformer (18 kV, alternating current with a frequency of 250 Hz). The ceramic tubes are inserted in an aluminum housing which is connected to the ground. A silent discharge is generated in the oxygen flow, which produces 1.5×10^{19} molecules min $^{-1}$ of O_3 . The pressure in the discharge tube is kept constant between 1 and 1.2 bar and is monitored by a pressure transducer. More details are described by Volz-Thomas et al. (2005).

2.1.4 Photolytic converter

The photolytic converter (PLC) consists of a UV transparent borosilicate glass tube (25 mL), which is mounted behind the manifold. The tube is illuminated by four UV-light-emitting diodes (UV-LEDs, 395 ± 5 nm, 250 mA, 5 VA each, 20 VA total) to convert NO₂ in the sample air into NO by absorption of a UV photon. The UV-LEDs and the associated power transistors of the LED power supply are mounted on individual heat sinks, which are cooled by air entering through the bottom of the housing by means of an external fan. Laboratory tests showed that the air passing the PLC is heated by about $30\,^{\circ}\text{C}$ above the instrument temperature if the UV-LEDs are switched on (Fig. 3). The determination of the converter efficiency and the NO₂ photolysis frequency (J_{PLC}) of the UV-LEDs are shown in Sect. 2.2. Possible interferences are discussed in Sect. 4.

2.1.5 The inlet line, exhaust line and inlet manifold

The inlet line consists of a 90 cm long PFA tube with an outer diameter (OD) of 1/8 in. It starts in the Rosemount housing outside of the fuselage of the aircraft (Nédélec et al., 2015) and ends at the inlet manifold of the NO_x instrument. The residence time within the inlet line is about 0.05 s; thus, losses due to the reaction of NO and O_3 to NO_2 are negligible. About 10% (150 mL min⁻¹) of the total inlet flow is sucked from the manifold into the analytic section of the instrument by means of two membrane pumps (Vacuubrand MD1) operated in parallel. The flow is regulated by a mass flow controller (Bronkhorst, IQF-200-AAD-00-V-S). The excess of the inlet flow is flushed through the exhaust

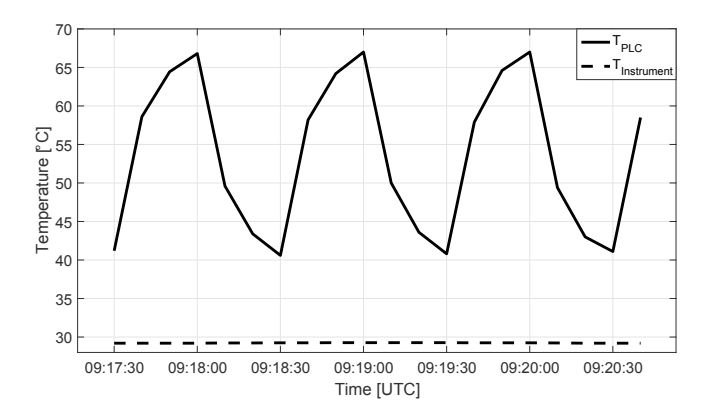


Figure 3. Gas temperature in the photolytic converter and instrument temperature measured in the laboratory when switching the UV-LEDs on and off every 30 s.

line, which starts at the end of the inlet manifold, provided with an exhaust manifold to gather all flows (e.g., internal calibrations) which have passed through the instrument. Outside the instrument the excess flow is guided through the exhaust line (PTFE tube of 60 cm length with 6 mm outer diameter) to the outlet port at the fuselage of the aircraft. The manifold is made of stainless steel and contains ports for pressure measurement and for the addition of zero air and calibration gas. The total residence time from the manifold to the NOD is between 2.5 s at cruising altitude and 12 s at sea level. Thus NO losses by Reaction (R1) with ozone in the ambient air need to be accounted for when the LEDs of the photolytic converter are switched off.

2.1.6 Instrument response characterizing

The response time of the instrument is important for the correction of NO titration by ambient O_3 during sampling and by fast changes of the ambient conditions (e.g., the aircraft crosses the tropopause). The response time of the instrument was characterized in the laboratory by repeating 10 injections of 2 s NO pulses of 7.1 ppbv into the inlet line at each full minute at 250 hPa inlet pressures (Fig. 4). The width (1/e) of the NO peak is 4 s, which represents a peak broadening of a factor of 2, and the delay is about 3 s at an inlet pressure of 250 hPa.

2.1.7 Internal stability checks

Inside the instrument, NO₂ is continuously produced from a permeation tube (PT, KIN-Tek, EL-SRT2-W-67.12-2002/U) placed inside a stainless-steel block, which is purged with a small flow (<12 mL min $^{-1}$) of oxygen (Revision 1) or synthetic air (Revision 2). The stainless-steel block is temperature-controlled at $40\pm0.5\,^{\circ}\mathrm{C}$ using a Pt100 sensor and PID controller. The NO₂ flow enters the inlet manifold and is only used for stability checks of the detector sensitivity. During flight, the calibration gas is normally pumped

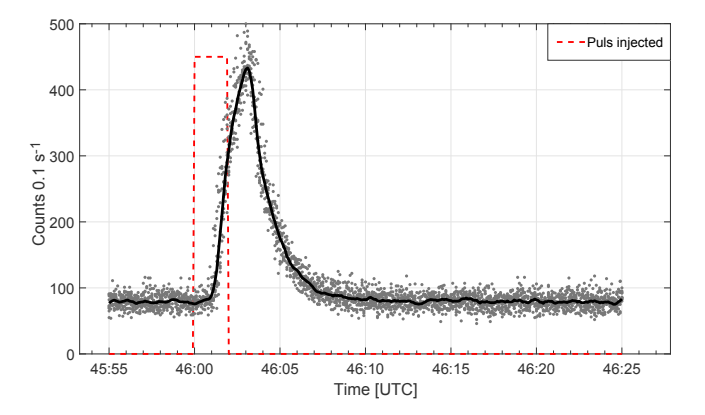


Figure 4. 10 repetitions of the NO pulse (red, dashed) experiment covering 30 s time period. The NO pulse (7.1 ppb) was injected for 2 s directly into the inlet line at each full minute at inlet pressure of 250 hPa. The pulse response (black line) is smooth with a running mean (2 s). The width (1/e) of the peak is 4 s, and the delay is about 3 s.

away through the exhaust and will not reach the sample flow. If this pump flow is disabled, the calibration gas will reach the analytic section for a stability check of about 5 min duration (Fig. 5).

2.1.8 Instrument operation

The IAGOS NO_x instrument is designed for autonomous deployment over several months. It is synchronized during flight with the main package, P1. The time synchronization has been cross-checked using the ozone measurements from P1, which are also transferred every 4 s to the P2 instrument during operation mode. The software utilizes aircraft signals (currently weight on wheels) to switch between operation mode during flight and standby mode on the ground. The instrument operates in a strict cyclic way by switching the PLC on (NO_c mode) or off (NO mode) and by flushing the air into the pre-chamber or directly into the reaction cell. During normal operation in flight the ambient air along the flight track is sampled. In addition to the PMT signal (recorded in 10 Hz), pressures, sample flow and temperatures at different positions are recorded as 1 min averages to monitor the state of the instrument. For in-flight system checks, the manifold is flushed in regular intervals with NO_x -free gas or NO_2 calibration gas (approximately 10-15 ppbv, generated from a permeation tube). On the ground, the instrument is in standby mode and does not record data. The ozone generator (O3G) is switched off, and the valves to the pump and between manifold and exhaust are closed, which leads to a backward flow of synthetic air from the gas bottles through O3G, NOD and manifold to the inlet, in order to avoid contamination by polluted air at the airport. The different modes of the instrument are summarized in Table 3, and the cyclic measurements during flight are shown in Fig. 5.

2.2 Calibration

The detector sensitivity, the conversion efficiency and the photolysis rate coefficient are determined by external calibrations in the laboratory using procedures defined in the standard operating procedure (SOP) for P2b (see http:// www.iagos.org/iagos-core-instruments/package2b/, last access: 29 November 2017) and described in detail in the following subsections. In principle, the instrument is flushed with a known mixture of NO and synthetic air, and NO₂ produced by gas-phase titration (GPT). The mixing ratio is calculated from the measured flows of the NO calibration gas, oxygen and NO_x -free zero air (see Sect. 2.2.3). The titration rate of the external GPT mixture is adjusted to 70-90 %. A simplified example of one calibration is shown in Fig. S2 in the Supplement. Note that the entire calibration procedure is performed at 250 hPa inlet pressure. Table 4 shows the uncertainties of laboratory calibrations for the deployment phases in 2015 and 2016.

2.2.1 NO detector sensitivity

The detector sensitivity (S_{NOD}) is determined from the photon count rates (CAL_{NO}) by flushing the instrument with a mixture of known NO mixing ratio (μNO) from the secondary standard $(NO_{Standard})$, synthetic air (SL) and oxygen (O_2) :

$$S_{\text{NOD}} = \frac{\text{CAL}_{\text{NO}}}{\mu \text{NO}},\tag{2}$$

where

$$\mu \text{NO} = \text{NO}_{\text{Standard}} \times \frac{\text{flow}_{\text{NO}}}{\text{flow}_{\text{NO}} + \text{flow}_{\text{O2}}}.$$
 (3)

Our NO working gas standard (10 ppmv NO mixed in N_2 , 5.0) is a secondary standard and is regularly referenced to the primary standard of the World Calibration Center for NO_x at the Forschungszentrum Jülich. Up to now, deviations between both standards have been found to be smaller than 1%. The uncertainty of the flow measurements is below 2%. The uncertainty of the detector sensitivity (δS_{NOD}) from the calibrations is 2 to 3%, accounting for the errors of the flow meters and the primary NO standard. As an example, for a detector sensitivity of 1000 cps ppt⁻¹ the uncertainty is 30 cps ppt^{-1} .

2.2.2 NO₂ conversion efficiency and the NO₂ photolysis frequency

The conversion efficiency (E_{PLC}) is calculated from the measured NO and NO_x signals during the calibration by external GPT (CAL_{GPT}) by switching the UV-LEDs in the PLC on and off (Table 3). Note that the instrument background using NO_x-free gas and the signals from the pre-volume (zero mode) must be subtracted from all signals in measuring mode

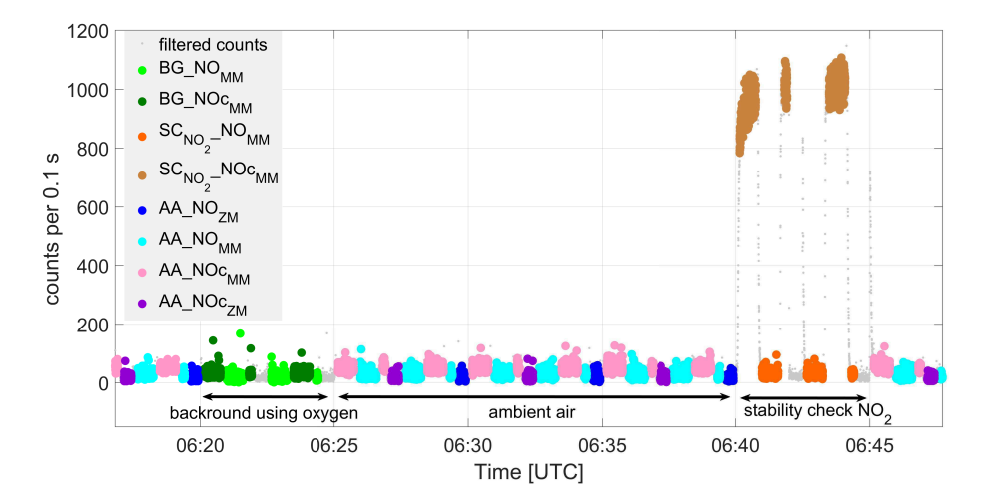


Figure 5. Example for the in-flight measurement cycle. The different modes of the instrument are denoted by horizontal arrows: in ambient air the measuring modes (MM) are shown for NO_c (light red) and NO (light blue); the zero modes (ZM) are shown for NO_c (purple) and for NO (dark blue). The instrument background checks are made using a zero-air gas bottle supply and are shown for NO_c (dark green) and for NO (light green). Stability check: NO_2 produced by the internal calibration source (permeation tube) is shown for NO_c (brown) and for NO (orange). The gray dots show discarded data during switching between the different modes.

(see Sect. 3):

$$E_{\rm PLC} = \frac{\rm CAL_{\rm GPT}NO_{\rm c} - \rm CAL_{\rm GPT}NO}{\rm CAL_{\rm NO}NO - \rm CAL_{\rm GPT}NO}. \tag{4}$$

Typically, the conversion efficiency is between 75 and 85 %, depending on the ambient pressure. During a deployment period of 6 months the total uncertainty of the conversion efficiency is determined within 4 %.

The photolysis frequency (j_{PLC}) of the UV- LEDs is calculated as follows:

$$j_{\rm PLC} = \frac{-\ln\left(1 - E_{\rm PLC}\right)}{\tau},\tag{5}$$

with τ being the residence time in the converter. The photolysis frequency of the UV-LEDs was stable at $j_{PLC} = 0.55$ (± 0.05) s⁻¹ during the last eight pre- and post-calibrations at inlet pressure of 250 hPa. During flight, this value is used to calculate for each measured data point the conversion efficiency considering the residence time and the ambient pressure in the converter.

2.2.3 Zero air (NO_x -free air)

In the laboratory zero air is generated using one of the following:

- a. dried and purified compressed air using a Parker Hannifin adsorption dryer (dewpoint temperature $T_{\rm d} < -40\,^{\circ}{\rm C}$) and an additional active charcoal filter for removing NO_x, ozone and volatile organic compounds (VOCs);
- b. pure O_2 (99.5%) from gas bottles, which is also used for the ozone generator;

c. synthetic air (Air Liquide).

The three zero-air types showed no differences in zero mode within measurement errors, which is in agreement with the finding of Volz-Thomas et al. (2005) for the MOZAIC NO_y instrument. However, the difference between measuring mode and zero mode of instrument background signal is not equal to zero and has to be subtracted from the ambient measured signal (see Sect. 3).

2.3 Quality assurance

Within the IAGOS community it was agreed to flag data quality according to the criteria elaborated in the EU Seventh Framework Programme (FP7) project IGAS (IAGOS for the GMES Atmospheric Service; http://igas-project.org, last access: 29 November 2017; Gerbig et al., 2014). One major topic of this project was to develop QA and quality control (QC) rules, defined in SOPs in collaboration with the IAGOS user community. The flagging criteria are summarized in Table 5. Quality assurance is performed according to the SOP for P2b and is described briefly in the following. Shortly, before and after each deployment period, the entire instrument performance is checked, and necessary replacements or services of compounds are performed, based on the expected lifetime of parts or due to deteriorated performance.

The calibration procedure includes

- determination of the detector sensitivity for NO and the conversion efficiency for NO₂ of the PLC using an external calibration setup with GPT;
- determination of the instrument background with internal zero air and external zero-air supply;

Table 3. Definition of the different modes of the instruments and their acronyms; note some of the modes are not used during flight.

Air supply	UV-LEDs	Name of the modes	Comment		
Ambient air	Off	AA_NO _{MM}	Ambient NO is measured by reaction with O ₃ in the reaction cell		
		AA_NO _{ZM}	About 98 % of ambient NO is oxidized in the pre-volume to determine the background signals from other chemical reactions		
	On	AA_NOc _{MM}	Ambient NO_x (NO + NO ₂ photolytic reduced) is measured by reaction with O_3 in the reaction vessel		
		AA_NOc _{ZM}	Same as above, flushing the air into the pre-volume		
Determine instrument back- ground using pure O ₂ or syn- thetic air	Off	BG_NO _{MM}	Bottled synthetic air (Rev. 2 instruments) or pure O_2 (Rev. 1 instruments) is sucked into the instrument to determine the background signal for NO_x -free gas of the instrument during flight		
		BG_NO _{ZM}	Same as above, flushing the air into the pre-volume		
	On	BG_NOc _{MM}	Bottled synthetic air or pure O_2 is sucked into the instrument in the reaction vessel to determine the background signal for NO_x -free gas of the instrument during flight		
		BG_NOc_{ZM}	Same as above, flushing the air into the pre-volume		
Instrumental stability check for NO or NO ₂	Off	SC_NO _{MM}	Synthetic air (or pure O ₂) is flushed through a heated (40 °C) permutation tube and mixed with the ambient air in the manifold before it is sucked into the instrument directly on the reaction vessel		
		SC_NO _{ZM}	Same as above, flushing the air into the pre-volume		
	On	SC_NOc _{MM}	Synthetic air (or pure O ₂) is flushed through a heated (40 °C) permutation tube and mixed with the ambient air in the manifold before it is sucked into the instrument directly on the reaction vessel		
		SC_NOc _{ZM}	Same as above, flushing the air into the pre-volume		
Instrument calibration using external gas supplies only in the laboratory	Off	Cal_NO _{MM}	Different types of gases (NO, NO ₂ or NO _{x} -free) can be flushed into the inlet line before being sucked into the reaction chamber		
•		Cal_NO _{ZM}	Same as above, flushing the air into the pre-volume		
	On	Cal_NOc _{MM}	Different types of gases (NO, NO ₂ or NO _{x} -free) can be flushed into the inlet line before being sucked into the reaction chamber		
		Cal_NOc _{ZM}	Same as above, flushing the air into the pre-volume		

Table 4. Overview of the calibration uncertainties for the two deployment phases in 2015 and 2016.

2015	2016
< 5 %	<4%
< 2 %	< 3 %
< 1 %	
NO < 10 pptv;	$NO_2 < 20 \text{ pptv}$
	<5 % <2 % <1 %

 calibration of pressure sensors, capillaries and flowcontrollers.

Additionally, the in situ NO measurements are used as an in-flight quality check of the instrument since NO is completely oxidized to NO_2 during nighttime, and its mixing ratio should be 0 pptv (see results in Sect. 5). Internal NO_2 calibrations are used to monitor the NO detector sensitivity during the deployment (see Sect. 4.1). Regular instrument intercomparison with state-of-the-art instruments is performed to determine the uncertainty of the instrument (see Sect. 4.2), which includes case studies for NO_2 -containing species and their possible interferences (see Sect. 4.3).

Table 5. Criteria for flagging the NO_x data according to QA/QC definition in IGAS (www.igas-project.org).

	Value	Comment
Good	0	
Limited	2	PMT temperature is larger than -5 °C; ozone correction not possible; water vapor correction not possible; large variation of internal stability checks.
Erroneous	3	Measurements below the detection limit; NO nighttime values enhanced; in situ zero-air measurements are enhanced; PMT temperature is larger than 10 °C.
Not validated	4	Non-validated data points (e.g., NO ₂ > 4 ppbv at cruising altitude), ascent profile (heating up of the instrument units, e.g., ozone generator).
Missing value	7	Cyclic measurement of NO and NO_x , zero mode, internal calibrations

3 Data processing

3.1 From raw signal to mixing ratio

The following steps describe briefly how the mixing ratios of NO, NO₂ and NO_x are calculated from the different instrument mode signals (PMT count rates) for each flight:

- Interpolate a time series of the different zero mode signals (AA_NOc_{ZM} or AA_NO_{ZM}) separately by using a running mean with a window size of 400 s. This time frame covers at least four NO_c and NO mode cycles with the current setup and determines the baseline. The running mean was chosen because it performed best at the beginning and the end of the time series compared to other interpolation methods.
- 2. Subtract the interpolated zero mode signal from the measuring mode signals (ambient air, zero air etc).
- 3. Subtract the instrumental background signals (BG_NO_{MM} and BG_NOc_{MM}) from the ambient measurement signals (AA_NO_{MM} and AA_NOc_{MM}) to avoid artifact signals (Drummond et al., 1985).
- 4. Calculate ambient NO mixing ratio ([NO]_{AA}) by applying Eqs. (1) and (2), where $S_{\text{NOD}}(t)$ is the time-dependent detector sensitivity (determined in the laboratory before installation and after deinstallation). $S_{\text{NOD}}(t)$ slightly decreases with time (see Sect. 4).

$$[NO]_{AA} = \frac{AA_NO_{MM}}{S_{NOD}(t)}$$
 (6)

Calculate the ambient NO₂ and NO_x mixing ratios using the detector sensitivity $S_{\text{NOD}}(t)$, the converter efficiency E_{PLC} and the median NO mixing ratio (before

and after each NO_x measurement) by applying Eqs. (1), (2), (5) and (6):

$$[NO_2]_{AA} = \frac{AA_NOc_{MM} - AA_NO_{MM}}{S_{NOD}(t) \times E_{PLC}(t)}$$
(7)

$$[NO_x]_{AA} = [NO]_{AA} + [NO_2]_{AA}$$
 (8)

- 5. Apply the water vapor and ozone corrections using Eqs. (9), (10) and (11) (see below).
- 6. Use nighttime NO measurements to correct possible offsets associated with the zero mode. Nighttime periods are identified using the actual position of the aircraft, time and altitude, by calculating the solar zenith angle. Angles larger 100° are used to flag the data as nighttime. Daytime measurements are flagged using solar zenith angles <80°. In between, the measurements are within the twilight zone, where NO is not fully oxidized by ozone.
- 7. Flag each data point according to Table 5.
- 8. The data time resolution is provided at 4 s by calculating the median based on 10 Hz raw data for the individual four second periods to be consistent with the other measured compound time series within IAGOS. The time resolution corresponds therefore to a horizontal resolution of approximately 1 km at cruising altitude. We used the median of the corresponding time interval to avoid a statistical bias uncertainty (Yang et al., 2004).

3.1.1 Water vapor correction

The third-body quenching effect of water vapor molecules on the excited NO_2 molecules in the reaction chamber leads to a reduced signal depending on the amount of ambient water (Parrish et al., 1990; Ridley et al., 1992). The correction factor has to be applied using Eq. (9):

$$[NO_{corr}]_{AA} = [NO]_{AA} \times (1 + \alpha \times [H_2O]), \tag{9}$$

with $[H_2O]$ being the water vapor mixing ratio in parts per thousand. In the laboratory we determined the humidity interference parameter of $\alpha = (2.8 \pm 0.1) \times 10^{-3}$, independent of whether the PLC was switched on or off, which is 35% lower than the value of $\alpha = 4.3 \times 10^{-3}$ determined by Ridley et al. (1992). Most of the IAGOS data are obtained at cruising altitude, where $[H_2O]$ is in the range of <5 to 100 ppmv. Under these conditions, the water vapor interference is negligible. Within the planetary boundary layer, especially in the tropics, the $[H_2O]$ can reach values of several thousand ppmv, leading to an interference of up to 10% (Fig. S4). If a water vapor correction could not be applied (e.g., missing water vapor measurements), then the data within the PBL (lowest: 3 km above ground) are flagged as "limited" (Table 5).

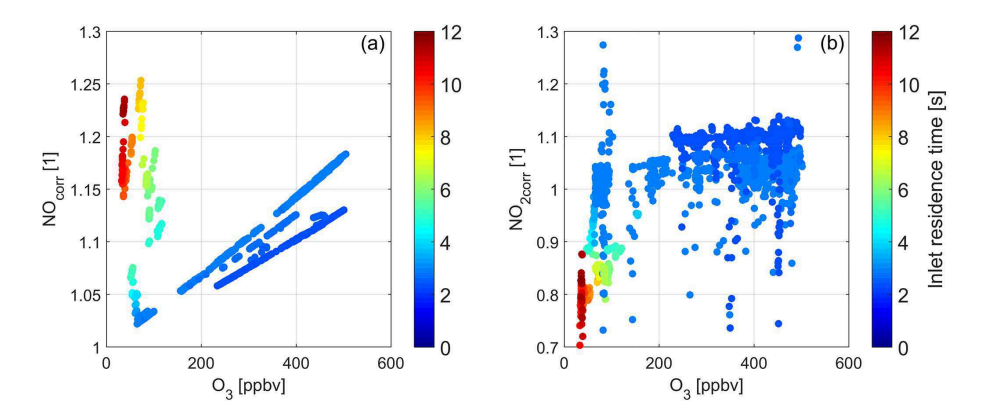


Figure 6. Typical correction factors for (a) NO and (b) NO₂, which depend on ambient ozone and residence time (color bar) in the inlet manifold system, for one flight from DUS to NYC in June 2015.

3.1.2 Ozone correction

Within the sample line and the converter, Reaction (R1) is still active. Depending on the residence time the reaction will lead to an enhanced NO₂ / NO ratio. The residence time (τ) in the inlet line is on the order of about 0.05 s, and corrections are negligible here. The residence time of the constant sample mass flow within the PLC is about $\tau = 2.5$ to 12 s as a function of the ambient pressure. The ozone corrections are applied using the in situ ozone measurements from Package 1 and the photolysis frequency J_{PLC} of the UV-LEDs (see Eqs. 5–7) as described in the SOP for NO_x from AC-TRIS.

$$[NO]_{0} = [NO]_{AA} \times \exp(k_{O_{3}} \times \tau)$$

$$[NO_{2}]_{0} = \left(\frac{J_{PLC} + k_{O_{3}}}{J_{PLC}}\right)$$

$$\times \frac{[NO_{c}]_{AA} - [NO]_{AA} \times \exp(-J_{PLC} \times \tau)}{1 - \exp(-(k_{O_{3}} + J_{PLC}) \times \tau)} - [NO]_{0}$$
 (11)

Here [NO]₀ ([NO₂]₀) is the expected mixing ratio at the entrance of the Rosemount inlet, and [NO]AA ([NO2]AA) is the calculated mixing ratio using the photon count rate, photolysis frequency of the NO2 converter and NO detector sensitivity (see Sect. 2.2). The factor k_{O_3} (= $k \times [O_3]$) is calculated from the reaction constant for Reaction (R1) $(k = 1.4 \times 10^{-12} \times e^{-1310/T}$; Atkinson et al., 2004) and the ozone concentration (ccm^{-3}), which is calculated from the in situ measured ozone mixing ratio measured by the IAGOS P1 instrument and the ambient pressure. Figure 6 shows the correction factor for NO $(NO_{corr} = [NO]_0 / [NO]_{AA})$ and for NO_2 ($NO_{2corr} = [NO_2]_0 / [NO_2]_{AA}$). NO increases by up to 25 %, and NO₂ varies in the range ± 10 %, both depending on the ambient mixing ratio of ozone, temperature and pressure. Since the ozone correction is sensitive to the ozone mixing ratio, the residence time τ inside the PLC is determined for each instrument for the expected pressure range from 1000 to 180 hPa, which provides the correction function $\tau(p)$ to be used in Eqs. (10) and (11) (see Fig. S5). For the future generation of IAGOS NO_x instruments, we plan to keep the residence time in the PLC at 3 s, independent from the inlet pressure, by using a critical nozzle.

3.2 Instrument uncertainty

3.2.1 Signal precision and limit of detection

The precision of the instrument is limited by the dark noise of the PMT caused by counting thermal radiation photons. The counting statistic is Poisson distributed. The background signal is subtracted from the ambient signal (see Sect. 3.1). Therefore, the limit of detection (LOD) is calculated from the 2σ statistical precision of the zero-air measurements in measuring mode (BG_{O2}_NO_{MM}) and zero mode (BG_{O2}_NO_{ZM}), which are integrated over 4 s (t=4 s) following Feigl (1998):

$$LOD_{NO} = \frac{2}{S_{NOD}}$$

$$\times \left(\sqrt{\frac{BG_{O_2} - NO_{MM}}{t}} + \sqrt{\frac{BG_{O_2} - NO_{ZM}}{t}} \right), \qquad (12)$$

$$LOD_{NO_c} = \frac{2}{E_{PLC} \times S_{NOD}}$$

$$\times \left(\sqrt{\frac{BG_{O_2} - NO_{cMM}}{t}} + \sqrt{\frac{BG_{O_2} - NO_{cZM}}{t}} \right). \qquad (13)$$

Here the different count rates of the photons are given in counts per seconds (s⁻¹), and the unit of the instrument sensitivity is counts per second per pptv (cps pptv⁻¹). We derive a detection limit of LOD_{NO} = 24 pptv for NO and LOD_{NO2} = 35 pptv for NO₂ for 4 s integration time for a sensitivity of 0.9 cps pptv⁻¹. By integrating the data over 1 min, the detection limits improve to LOD_{NO} = 6 pptv and LOD_{NO2} = 9 pptv.

3.2.2 Total uncertainty

The total uncertainty for each measurement point is calculated by error propagation following from Eq. (1):

$$D_{\text{NO}} = \frac{1}{S_{\text{NOD}}} \times \left(\delta \text{MM} + \delta \text{ZM} + \delta \text{offset}\right) + (\text{MM} - \text{ZM} - \text{Offset}) \times \frac{\delta S_{\text{NOD}}}{S_{\text{NOD}}},$$

$$D_{\text{NO}_2} = \frac{1}{E_{\text{PLC}} S_{\text{NOD}}} \times \left(\delta \text{MMc} + \delta \text{ZMc} + \delta \text{offset}\right) + (\text{MMc} - \text{ZMc} - \text{Offset}) \times \left(\frac{\delta S_{\text{NOD}}}{S_{\text{NOD}}} + \frac{\delta E_{\text{PLC}}}{E_{\text{PLC}}}\right).$$
(15)

The uncertainty of the count rate in measuring mode (δ MM), zero mode (δ ZM) and offset (δ offset) is determined from the baseline noise for NO and NO_x measurements. Statistical precision (2σ) of an individual 4s data point is calculated by error propagation using Eqs. (4) and (5). The uncertainty of the detector sensitivity during calibration is 2 to 3 %, and the uncertainty of the converter efficiency is 4 to 5 %. Figure 7 shows the relative uncertainty (ratio of the total uncertainty to its measured value) as a function of NO and NO₂ in the range of observations during 2015. The relative uncertainty of an individual 4 s data point is dependent on the ambient mixing ratio and reaches NO values of 25 % at 0.2 ppbv and 8 % at 1 ppbv. For NO₂ the relative uncertainty is 50 and 18%, respectively. Similar uncertainties were calculated for all observations in 2016. The total uncertainty in the low pptv range is mostly dominated by statistical precision of the signal detector.

4 Instrument performance

The quality of the IAGOS NO and NO_2 measurements depends on the knowledge of the detector sensitivity during the flight phase, the accuracy and precision of the instrument, and possible interferences. These issues are discussed in the following subsections.

4.1 Instrument performance drift during deployment

The IAGOS NO_x instrument regularly showed a negative drift of the detector sensitivity during each deployment period of two counts per ppbv per day. This sensitivity drift was related to a slow degradation of the surface of the reaction cell during the deployment period. The sensitivity losses were corrected by applying a robust linear fit interpolation of the sensitivity between the pre- and post-deployment calibrations. The robust linear interpolation is confirmed by the internal stability checks of NO_2 during the deployment phase (Fig. 8) and well documented from the MOZAIC NO_y measurements (Thomas et al., 2015). The internal stability checks of NO_2 , however, are not used for determining the

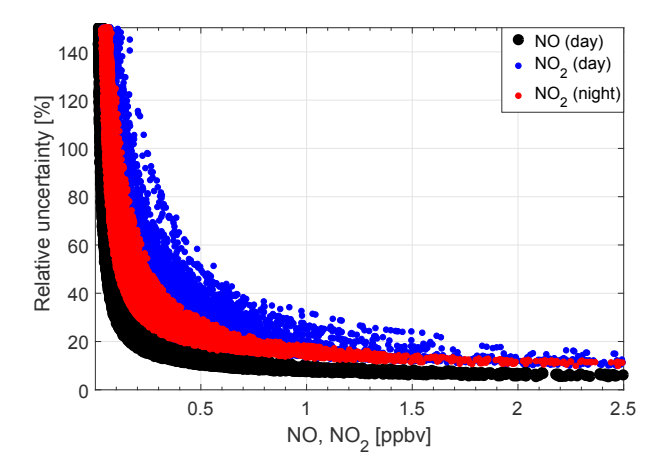


Figure 7. Relative uncertainty of NO (black, day) and of NO₂ (blue, day; red, night) using all measurements (4 s) in 2015.

mixing ratios from the raw signal. It should be noted that final data (L2) are provided after the post-calibration. Therefore the instrument operation period is kept short to a maximum of 6 months.

4.2 Instrument intercomparison

The German Weather Service organized an intercomparison of instruments measuring $NO/NO_2/NO_x$ mixing ratios within the framework of ACTRIS. Here 11 European laboratories participated with 17 different state-of-the-art NO, NO_2 and NO_x instruments during a 2-week period in October 2016. Most of the time all instruments agreed well, and the results of this workshop will provide detailed cross-sensitivities of each individual instrument compared to the reference CLD instrument of the World Calibration Center (WCC) NO_x . The WCC NO_x instrument (here after REF) was regularly calibrated during this campaign and is used as a reference.

Figure 9 shows correlations of NO and NO₂ for the IA-GOS NO_x and the REF instruments for ambient air measurements during 2 days of this campaign. The ambient air was distributed by a ring line of 20 m length, with residence times of approximately 5 to 6 s from the first to the last instrument and corrected for ambient ozone mixing ratio. Mixing ratios of NO were observed in the range of the detection limit and 6 ppbv. The correlation coefficient is higher than $R^2 > 0.98$ with a slope of 1.037 and an offset of -18 pptv. NO₂ was observed in the range of 0.5 to 10 ppbv with $R^2 > 0.94$ with a slope of 1.063 and an offset of -102 pptv. The NO₂ data are more scattered than NO data, which is related to the different cyclic measurements of NO and NO₂ by both instruments. Further results (e.g., chemical interferences) will be presented in a separate paper. This and future intercomparisons will assure the quality of the IAGOS NO_x instrument.

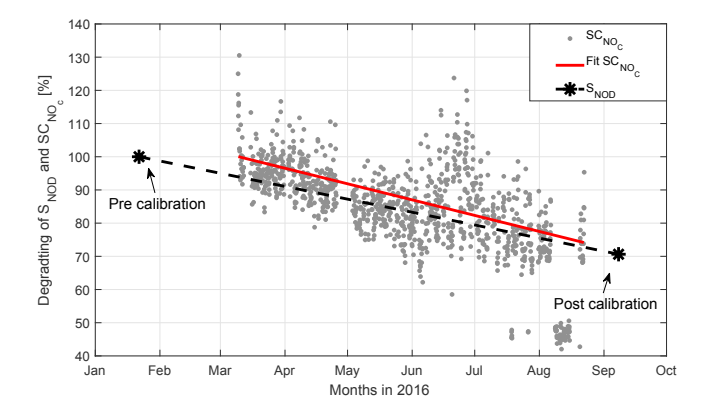


Figure 8. Linear degrading of the NO detector sensitivity (S_{NOD} , black) after pre- and post-calibration in percent. The in-flight stability check of NO_2 (gray dots) confirms the linear behavior of the degradation of the detector sensitivity during the deployment, shown as linear robust fit (red line).

4.3 Possible interferences

4.3.1 Photolytic decomposition

It is known that photolytic decomposition of nitrous acid (HONO) can occur when using a photolytic converter for the detection of NO_2 with CLD instruments (e.g., Fehsenfeld et al., 1990). During the ACTRIS NO_x side-by-side intercomparison the interference of HONO within the IAGOS NO_x instrument was determined to be about 10% of the NO measurements at 11 ppbv. In situ observations of HONO in the UTLS regions are very rare, and they report only a few ppt (Jurkat et al., 2011, 2016). Thus, the interferences are mostly below the total uncertainties for NO and NO_x . This is also the case for BrONO₂ and NO_3 . Both species can be decomposed within the photolytic converter. The concentrations of both species are too low (< 10 ppt) in the UTLS region; thus we expect no major impact on the NO_2 measurements (Avallone et al., 1995; Brown et al., 2007; Carslaw et al., 1997).

4.3.2 Thermal decomposition of NO₂-containing species

The instrument temperature is measured and varies mostly between 15 and 22 °C during flight. With the aircraft being close to the ground, the instrument temperature can rise up to 30 °C in summer. However, the gas temperature inside the PLC increases when the LEDs are switched on. Laboratory measurements showed that the gas temperature in the converter is in the range of 40 to 70 °C at an instrument temperature of 30 to 35 °C (Fig. 3). From these experiments, we extrapolate a gas temperature inside the converter between 27 °C (300 K) and 47 °C (320 K) during flight. As a result, thermal decomposition of reservoir species containing NO₂ can lead to erroneously enhanced NO₂ measurements. Reed et al. (2016) showed that the PAN interference could be up

to 8 and 25 % when using an actively cooled and a not actively cooled photolytic converter, respectively. In the laboratory, we found NO₂ enhancements of 30 % by mixing PAN with the sample flow (at 35 °C instrument temperature and pressure level of 250 hPa), which was quantitatively generated from a NO calibration gas by photolysis of acetone (100 ppbv) in a flow system (Pätz et al., 2002; Volz-Thomas et al., 2002). The result is in good agreement with theoretical calculations of the lifetime of PAN at the maximum expected temperature of 340 K (at 250 hPa) in the PLC, which predicts an interference of 27 % to NO₂. However, temperatures in the PLC above 320 K are not expected during flight, because instrument and unit temperatures are much lower than in the laboratory, and thus PAN interferences should be less than 3 % for NO₂. Table 6 provides an overview of possible interference to the NO₂ measurements over different temperature ranges of the typical reservoir species containing NO₂ (dinitrogen pentoxide (N₂O₅), peroxynitric acid (HO₂NO₂, only during daytime), methyl peroxy nitrate (CH₃O₂NO₂), and peroxyacetyl nitrate (= PAN, CH₃CO₃NO₂)) at cruising altitude (250 hPa).

5 First results of NO, NO₂ and NO_x observations during in-flight operation

Nitrogen oxide measurements were obtained from two flight phases on board the Lufthansa Airbus A340-300. The compiled flight tracks are shown for both years in Fig. 10. The aircraft conducted 262 flights in 2015, mostly on routes across the North Atlantic (Düsseldorf-New York or Chicago). In 2016, 208 flights were performed while most flights were on routes from Germany (Frankfurt am Main) to South America (Bogota or Caracas) and various destinations in East and Southeast Asia. In 2015, data of 62 flights are missing due to instrument shutdown because of malfunctioning of system components. Only 10 flights are missing in 2016. In total, about 400 h of data are available in 2015, and 470 h of data in 2016. The relative amount of the archived measurements with the respective validation flag for all flights is summarized in Table 7. At this stage, parts of the IAGOS measurements are available only as L1 data (preliminary), which explains the large fraction of limited data in 2016. Progression of the data to L2 (final) is ongoing. Here, we show the first results as examples, to demonstrate the performance of the instrument. A detailed analysis will be presented in a separate paper once all data are finalized.

5.1 NO and NO₂ partitioning in the UTLS region

Figure 11 shows the NO and NO₂ mixing ratio probability density functions during all nighttime flights at cruising altitude ($p < 350 \,\text{hPa}$). The NO mixing ratio is expected to be zero within the standard deviation (1σ) of 25 pptv, which is equal to the statistical precision of the instrument at 4 s time

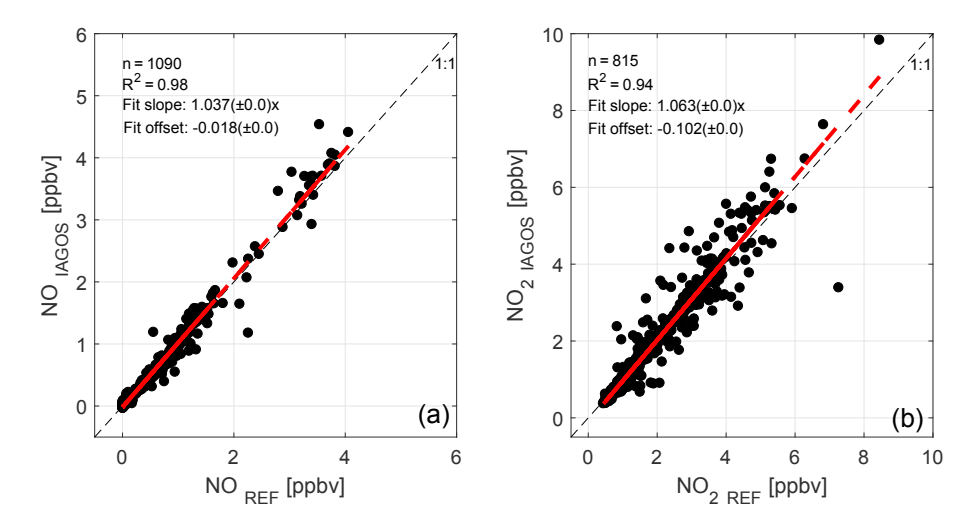


Figure 9. Two days of ambient NO and NO₂ measurements on Hohenpeißenberg in Germany in October 2016 during the ACTRIS NO_x instrument intercomparison. The data were averaged to 1 min means; no ozone or humidity correction were applied. The reference instrument (REF) was regulary calibrated during the campaign.

Table 6. Lifetime, mixing ratio and possible interferences of thermally decomposed reservoir species over different temperature ranges. Values in bold font indicate the most plausible temperature within the NO₂ converter in the IAGOS instrument during flight.

Species	Lifetime of the reservoir species at 250 hPa in s			Interference to NO ₂ at 250 hPa in %			Mixing ratio at cruising altitude (source)	
	300 K	320 K	340 K	300 K	320 K	340 K		
N_2O_5	23.9	2.6	0.4	11.8	68.4	100	<10 pptv (Brown et al., 2007)	
HO_2NO_2	27.1	2.9	0.4	10.5	64.0	100	< 66 pptv (Kim et al., 2007)	
CH ₃ O ₂ NO ₂	1.0	0.1	0.0	94.5	100	100	< 15 pptv (Browne et al., 2011)	
$CH_3CO_3NO_2 = PAN$	1.9×10^{3}	110	9.4	0.16	2.7	27.4	300-600 ppbv (Fischer et al., 2014;	
							Moore and Remedios, 2010)	

Table 7. Relative amount of available 4 s data points (here NO_x) with respect to its validation flag for all flights in 2015 and 2016.

Year	Total number	Good (flag = 0)	Limited (flag = 2)	Error (flag = 3)	Invalid (flag = 4)
2015	3.6×10^5 4.2×10^5	71.7 %	17.5 %	3.0 %	7.8 %
2016		34.1 %	58.2 %	2.9 %	4.8 %

resolution. The quality of the IAGOS NO_x measurement is determined not only by the instrument precision but also by the homogeneity and representative of the climatological data set. Therefore, the NO measurements at nighttime are used as an additional quality check during each flight. Sometimes, a small negative NO offset is found (NO < -10 pptv), which occurs due to subtraction of the zero-air signal from the net signal at very low mixing ratios of NO and NO_x . However, the half width of the distribution is larger than the random noise of the detector, and therefore the NO mixing ratio offset value is assumed to be zero. The median mixing ratio of NO_2 is 138.6 pptv with a width range from 0 pptv to

several hundred pptv. A comparable nighttime median NO_2 value of 141 pptv was observed for the 2016 deployment period in the UTLS region. During daytime, NO recovers by the photochemical balance with NO_2 , which leads to a median distribution for NO mixing ratios of 57 pptv (86 pptv in 2016) and for NO_2 mixing ratios of 78 pptv (47 pptv). The sum of daytime NO and NO_2 mixing ratios in 2015 is only 1% smaller compared to the nighttime NO_2 median value, which is equivalent to NO_x . Differences of daytime NO and NO_2 mixing ratios between 2015 and 2016 are related to different flight routes and flight levels (Fig. 10).

The NO_x partitioning is now compared to previous observations obtained by NOXAR and by CARIBIC. Brunner et al. (2001) showed median NO_x values of around 140 pptv (96 pptv) for summer (autumn) in the UTLS region over the North Atlantic in 1995 and 1996. The authors calculated NO_x with the photochemical balance using only daytime observations of NO and ozone. These median NO_x values can be confirmed by splitting the IAGOS measurements in 2015 into summer (165 pptv) and autumn (84 pptv), where the differences between the NO_x median mixing ratios are less than

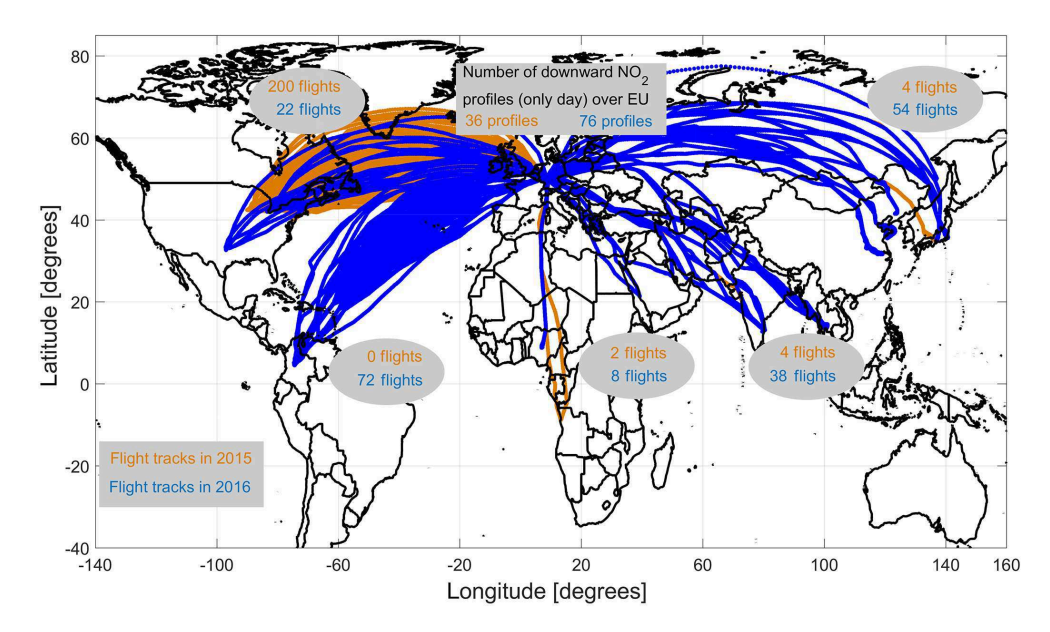


Figure 10. Flight tracks with the IAGOS NO_x instrument installed aboard the Lufthansa aircraft in 2015 and in 2016. Additionally, the amount of vertical profiles during day is denoted.

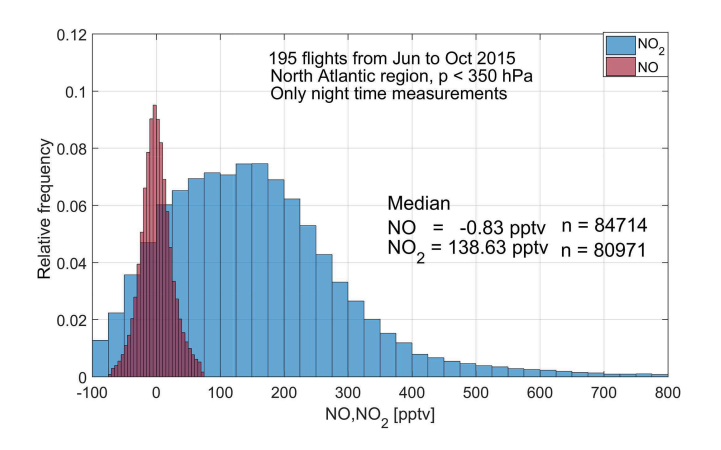


Figure 11. Relative frequency of nighttime NO and NO₂ measurements (4 s) at cruising altitude ($p < 350 \,\text{hPa}$) from 195 flights over the North Atlantic in 2015. The bin width is 25 pptv for NO₂ and 5 pptv for NO.

15 %. The NO_x values from CARIBIC are also calculated with the photochemical balance method, but using only day-time observations of NO and ozone, and considering only tropospheric air (Stratmann et al., 2016). In summer the median NO_x mixing ratio is close to 200 pptv, and in autumn 100 pptv, which is approximately 16 % larger than the values found in our IAGOS measurements.

The median of the IAGOS NO_x mixing ratios agrees well with the calculated median mixing ratios of NO_x from NOXAR and CARIBIC. However, previous studies identify an unexplained imbalance between the measured and calculated NO_2 in low- NO_x regions, which was explained by interferences of NO_2 -containing species and the large uncer-

tainty of the calculations (e.g., Crawford et al., 1996; Reed et al., 2016). Thus, the impact of interference from NO₂-containing species on the IAGOS measurements requires further investigations, which will be performed once a larger data set is available.

5.2 Discussion of observed features in the UTLS

As a first showcase of what can be gained from the IAGOS NO_x observations, Fig. 12 demonstrates a time series of all measured compounds for the flight from Düsseldorf to New York City on 23 August 2015. The measurements (CO, O₃, NO, NO₂ etc.) are presented as 2 min median averages to reduce the noise, and the potential vorticity (PV) was calculated using ECMWF (European Centre for Medium-Range Forecasts) ERA-Interim (Dee et al., 2011) data interpolated along the flight track (Berkes et al., 2017).

We want to focus now on the first more pronounced peak of NO_2 starting at $23:00\,\mathrm{UTC}$, where we suggest an intrusion of polluted air into the lowermost stratosphere. NO varies around 0 pptv during nighttime as expected, while a distinct strong peak of NO_2 is observed at $11.5\,\mathrm{km}$ altitude at $23:00\,\mathrm{UTC}$ which lasts for about an hour and is correlated with CO and relative humidity. The timely coincidence with high CO and H_2O values indicates that this air mass is highly polluted compared to typical mixing ratios at this altitude. This large peak is observed above the local tropopause, which can be identified by the chemical and dynamical tropopause heights. The chemical tropopause is often reported at $120\,\mathrm{ppbv}$ of ozone, and within the NO_2 plume the ozone mixing ratio is mostly larger than $150\,\mathrm{ppbv}$ (Thouret et al., 2006; Sprung and Zahn, 2010). The location

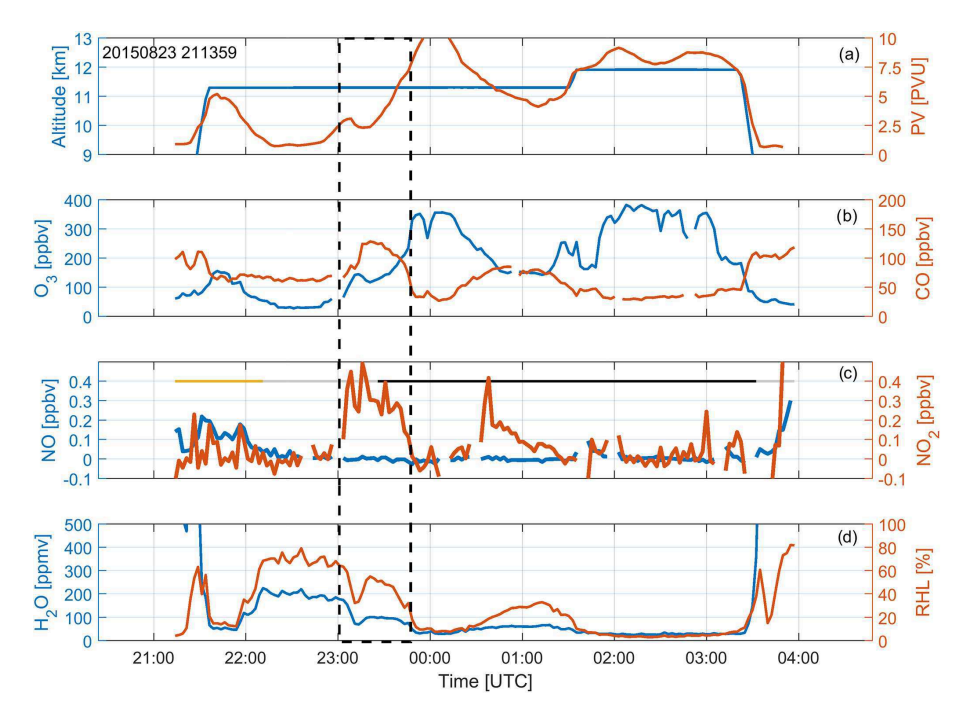


Figure 12. Time series of **(a)** flight altitude and PV, **(b)** ozone and CO, **(c)** NO and NO₂, and **(d)** H₂O and RHL from New York City (USA) to Düsseldorf (Germany) on 23 August 2015. The time of day is illustrated as a horizontal line (light orange: day; gray: sunset/sunrise; black: night). The shared black box shows a large-scale plume which is discussed in the text. All values are 2 min averages.

of the dynamical tropopause varies between 2.5 and $5\,PVU$ within the NO_2 plume, which is above the commonly used $2\,PVU$ defined location of the dynamical tropopause for the midlatitudes (Kunz et al., 2011).

The origin of this peak was identified using the Lagrangian transport model FLEXPART model. Here a rapid vertical transport from the surface by deep convection of a longrange-transported biomass burning plume could be identified. The FLEXPART model (version 9.02) was used to identify the region with the largest contribution from the surface using 5-day backward simulations from the particle dispersion (Stohl et al., 2005). FLEXPART results showed that a surface-based air mass was lifted from the northwestern US within the previous 4 days. Here near-surface emissions of NO and NO₂ from biomass burning could be identified using fire count maps from satellite images during that time (Fig. S3). These fire emissions contributed also largely to poor air quality in the mid-US at that time (Creamean et al., 2016; Lindaas et al., 2017). Further analyses are beyond the scope of this paper, but this showcase study already indicates the possibilities for air quality studies using the full amount of IAGOS observations.

5.3 Vertical profiles

Satellite column observations allow monitoring of NO₂ on a global scale, but the columns do not provide vertical resolution within the troposphere (although there have been recent cloud-slicing methods giving satellite NO₂ profiles on a cli-

matological basis), and the satellite retrieval depends on assumptions on the vertical distribution of NO_2 (Bucsela et al., 2008; Boersma et al., 2011; Veefkind et al., 2012). Laughner et al. (2016) showed that the estimates of NO_2 at the surface can be largely uncertain in regards to the daily meteorology if the a priori profile for NO_2 is not well known. So far, only a few methods exist to provide in situ NO_2 profiles, however with some limitations (e.g., Piters et al., 2012). We believe that this assumption can be evaluated with in situ vertical profiles of NO_2 from IAGOS to improve the satellite retrievals, which has been successfully demonstrated for CO (de Laat et al., 2014) and ozone (Zbinden et al., 2013).

In total, more than 400 descent profiles of nitrogen oxides are currently available over several regions in 2015 and 2016 (Fig. 10). Figure 13 shows the statistical analysis of NO and NO2 only at daytime over Düsseldorf Airport in summer (JJA) 2015. The vertical average was calculated in 50 hPa intervals from 200 to 1000 hPa. Median NO and NO2 values reach up to 200 pptv in the UTLS region (9-12 km), which agrees well with the previous observations over the eastern North Atlantic shown by Ziereis et al. (1999, 2000). The median NO and NO₂ values in the mid-troposphere (5 to 9 km), where no major sources exist, vary between the detection limit and 100 pptv. The largest values of nitrogen oxides are measured near the surface, with values up to several ppbv. It should be noted that these values represent a highly polluted region with a huge amount of emissions from ground traffic, industry and aviation. In further studies, the unique

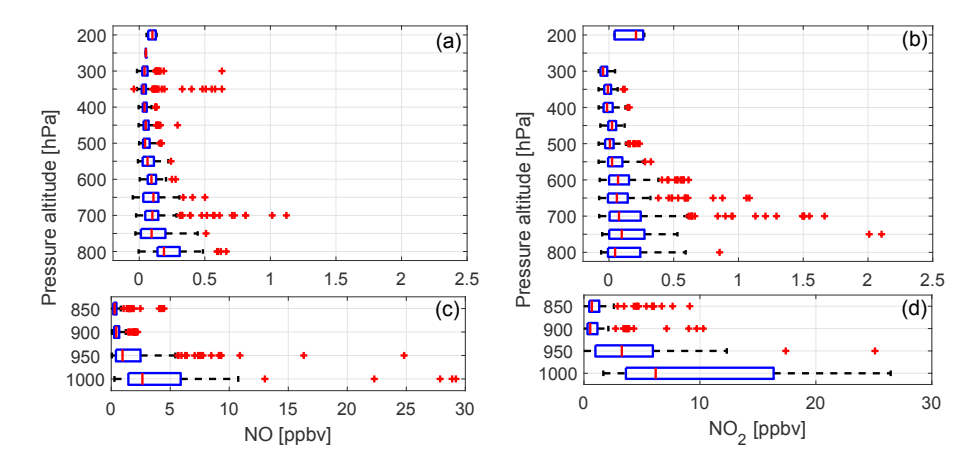


Figure 13. Statistical vertical distribution of NO and NO₂ (only at daytime) for (\mathbf{a}, \mathbf{c}) NO and (\mathbf{b}, \mathbf{d}) NO₂ over Düsseldorf Airport in summer (JJA) 2015. Note the different x-axis scale.

IAGOS NO₂ profiles will be used for a new satellite mission (TROPOMI, http://www.tropomi.eu, last access: 29 November 2017) and model evaluation (e.g., air quality).

6 Discussion and conclusion

The IAGOS NO_x instrument (P2b) setup provides measurements of nitrogen oxide with good precision and accuracy, while its design and performance are highly constrained by aircraft safety considerations and the requirement for unattended deployment over several months. We presented the different components and the determination of the uncertainties. The relative uncertainty of an individual 4 s data point is dependent on the ambient mixing ratio; for NO it reaches 25 % at 0.2 ppbv and 8 % at 1 ppbv, and for NO_2 it reaches 50 and 18 %, respectively.

So far only a few instruments are available which can be used for unattended aircraft observations over several months, because of the need of a high temporal resolution and a low detection limit and fulfillment of the safety requirements. The IAGOS NO_x instrument has a shorter residence time (at cruising altitude) and much larger conversion efficiency of NO₂ to NO than instruments using xenon lamps in the 1990s, which dramatically improves the instrument accuracy (Ryerson et al., 2000). The detection limit of the IAGOS NO_x instrument (LOD_{NO} = 24 pptv and $LOD_{NO_2} = 35$ pptv at 4 s, 2σ and 0.9 cps pptv⁻¹ detector sensitivity) is in the range of research-grade instruments used in research aircraft (e.g., CLD technique: $LOD_{NO} = 10$ to 50 pptv and $LOD_{NO_x} = 30$ to 80 pptv at 1 s (Pollack et al., 2012); CRDS technique, 1 s, 2σ : LOD_{NO} = 140 pptv and $LOD_{NO_2} = 90 \text{ pptv (Wagner et al., 2011)}.$

A major advantage of the IAGOS NO_x instrument is the provision of NO and NO_2 in situ measurements on a global scale with comprehensive seasonal and geographical coverage of the UTLS region, and the measurements of vertical

profiles from cruising altitude down to the surface over different continents. The emerging data set permits statistically robust conclusions on the seasonal and geographical distribution of NO_x . As a first example, the statistical analysis over the North Atlantic region shows lower median mixing ratios of NO and NO_2 in the UTLS compared to previous projects where NO_2 was determined with the photochemical balance, which is an indication that the possible interferences might be small if the amount of NO_x has not changed over the recent years.

Possible interferences for NO from HONO could be estimated to the order of 10%. The water vapor quenching effect on the NO signal was determined in the laboratory and is applied to the in situ measurements if water vapor measurements are available. Note that most of the time the aircraft samples in very dry air, where the correction is negligible. However, close to the surface the water vapor correction factor increases up to 10% at 30 000 ppmv. We apply to the measurements pressure- and temperature-dependent ozone corrections, which have large effects on NO (up to 25%). Thermal decomposition of NO₂-containing species might be a major source of uncertainty to the observed NO₂ mixing ratios. This also includes the blue-light converter, where we aim to reduce the temperature dependency while it is switched on and off within the next instrument revision.

The global distribution of NO_x in the UTLS region in combination with transport model calculation allows calculating impact ratios of anthropogenic compared to natural emissions and the concurrency of large-scale plumes. This will lead to a better understanding of the ozone chemistry in the highly climate-sensitive region of the UTLS. Vertical profiles of NO_2 show the expected C-shape profile, and the near-surface data can be used to monitor air quality in the vicinity of airports. Further, the day-to-day variations can be provided to improve satellite a priori profiles in the future (TROPOMI, http://www.tropomi.eu/, last access: 29 November 2017).

The current setup of the IAGOS NO_x instrument provided more than $800\,h$ of observations and 400 profiles using only one passenger aircraft as platform within 2 years (each 6 months). In the near future the number of aircraft will increase, leading to a larger statistical robustness of comprehensive seasonal and geographical coverage of in situ NO and NO_2 measurements.

Data availability. The data used in this study will be available from the central IAGOS database on the IAGOS website (http://www.iagos.org, last access: 29 November 2017.

The Supplement related to this article is available online at https://doi.org/10.5194/amt-11-3737-2018-supplement.

Competing interests. The authors declare that they have no conflict of interest.

Acknowledgements. The authors are grateful to Deutsche Lufthansa AG for providing special certification for the instrumentation on one A340-300, and in particular to Gerd Saueressig and to Markus Huf. We also thank enviscope GmbH, in particular Ralf Stosius and Gomolzig Flugzeug- und Maschinenbau for their excellent and continuous support within the IAGOS project. We gratefully acknowledge the continuous support by Andreas Volz-Thomas during the final development of the instrument and during the preparation of the manuscript. Without his fundamental work on the measurement of total odd nitrogen and nitrogen oxides in the MOZAIC and IAGOS programs, this instrument would not exist. Marlon Tappertzhofen, Torben Blomel, Marcel Berg, Benjamin Winter, Jennifer Gläser and Günther Rupsch are acknowledged for their enormous help in maintaining and calibrating the instrument. Dominik Brunner and Helmut Ziereis are acknowledged for fruitful discussions and as external reviewers for the SOP. Furthermore, we acknowledge ECMWF for providing meteorological analyses. Part of this project was funded by BMBF under IAGOS-D contract 01LK1301A. The IAGOS database is supported by AERIS (CNES and INSU-CNRS), where the IAGOS data are stored.

The article processing charges for this open-access publication were covered by a Research Centre of the Helmholtz Association.

Edited by: Folkert Boersma

Reviewed by: two anonymous referees

References

Ainsworth, E., Yendrek, C. R., Sitch, S., Collins, W. J., and Emberson, L. D.: The effects of tropospheric ozone on net primary

- productivity and implications for climate change, Annu. Rev. Plant Biol., 63, 637–61, https://doi.org/10.1146/annurev-arplant-042110-103829, 2012.
- Atkinson, R., Baulch, D. L., Cox, R. A., Crowley, J. N., Hampson, R. F., Hynes, R. G., Jenkin, M. E., Rossi, M. J., and Troe, J.: Evaluated kinetic and photochemical data for atmospheric chemistry: Volume I gas phase reactions of O_x , HO_x , NO_x and SO_x species, Atmos. Chem. Phys., 4, 1461–1738, https://doi.org/10.5194/acp-4-1461-2004, 2004.
- Avallone, L. M., Toohey, D. W., Schauffler, S. M., Pollock, W. H., Heidt, L. E., Atlas, E. L., and Chan, K. R.: In situ measurements of BrO During AASE II, Geophys. Res. Lett., 22, 831– 834, https://doi.org/10.1029/95GL00393, 1995.
- Berkes, F., Neis, P., Schultz, M. G., Bundke, U., Rohs, S., Smit, H. G. J., Wahner, A., Konopka, P., Boulanger, D., Nédélec, P., Thouret, V., and Petzold, A.: In situ temperature measurements in the upper troposphere and lowermost stratosphere from 2 decades of IAGOS long-term routine observation, Atmos. Chem. Phys., 17, 12495–12508, https://doi.org/10.5194/acp-17-12495-2017, 2017.
- Boersma, K. F., Eskes, H. J., Dirksen, R. J., van der A, R. J., Veefkind, J. P., Stammes, P., Huijnen, V., Kleipool, Q. L., Sneep, M., Claas, J., Leitão, J., Richter, A., Zhou, Y., and Brunner, D.: An improved tropospheric NO₂ column retrieval algorithm for the Ozone Monitoring Instrument, Atmos. Meas. Tech., 4, 1905– 1928, https://doi.org/10.5194/amt-4-1905-2011, 2011.
- Brenninkmeijer, C. A. M., Crutzen, P., Boumard, F., Dauer, T., Dix, B., Ebinghaus, R., Filippi, D., Fischer, H., Franke, H., Frieß, U., Heintzenberg, J., Helleis, F., Hermann, M., Kock, H. H., Koeppel, C., Lelieveld, J., Leuenberger, M., Martinsson, B. G., Miemczyk, S., Moret, H. P., Nguyen, H. N., Nyfeler, P., Oram, D., O'Sullivan, D., Penkett, S., Platt, U., Pupek, M., Ramonet, M., Randa, B., Reichelt, M., Rhee, T. S., Rohwer, J., Rosenfeld, K., Scharffe, D., Schlager, H., Schumann, U., Slemr, F., Sprung, D., Stock, P., Thaler, R., Valentino, F., van Velthoven, P., Waibel, A., Wandel, A., Waschitschek, K., Wiedensohler, A., Xueref-Remy, I., Zahn, A., Zech, U., and Ziereis, H.: Civil Aircraft for the regular investigation of the atmosphere based on an instrumented container: The new CARIBIC system, Atmos. Chem. Phys., 7, 4953–4976, https://doi.org/10.5194/acp-7-4953-2007, 2007.
- Brent, L. C., Thorn, W. J., Gupta, M., Leen, B., Stehr, J. W., He, H., Arkinson, H. L., Weinheimer, A., Garland, C., Pusede, S. E., Wooldridge, P. J., Cohen, R. C., and Dickerson, R. R.: Evaluation of the use of a commercially available cavity ringdown absorption spectrometer for measuring NO₂ in flight, and observations over the Mid-Atlantic States, during DISCOVER-AQ, J. Atmos. Chem., 72, 503–521, https://doi.org/10.1007/s10874-013-9265-6, 2015.
- Brown, S. S., Dubé, W. P., Osthoff, H. D., Stutz, J., Ryerson, T. B., Wollny, A. G., Brock, C. A., Warneke, C., de Gouw, J. A., Atlas, E., Neuman, J. A., Holloway, J. S., Lerner, B. M., Williams, E. J., Kuster, W. C., Goldan, P. D., Angevine, W. M., Trainer, M., Fehsenfeld, F. C., and Ravishankara, A. R.: Vertical profiles in NO₃ and N₂O₅ measured from an aircraft: Results from the NOAA P-3 and surface platforms during the New England Air Quality Study 2004, J. Geophys. Res., 112, D22304, https://doi.org/10.1029/2007JD008883, 2007.
- Browne, E. C., Perring, A. E., Wooldridge, P. J., Apel, E., Hall, S. R., Huey, L. G., Mao, J., Spencer, K. M., Clair, J. M. St.,

- Weinheimer, A. J., Wisthaler, A., and Cohen, R. C.: Global and regional effects of the photochemistry of CH₃O₂NO₂: evidence from ARCTAS, Atmos. Chem. Phys., 11, 4209–4219, https://doi.org/10.5194/acp-11-4209-2011, 2011.
- Brunner, D., Staehelin, J., Jeker, D., Wernli, H., and Schumann, U.: Nitrogen oxides and ozone in the tropopause region of the northern hemisphere: Measurements from commercial aircraft in 1995/1996 and 1997, J. Geophys. Res., 106, 27673, https://doi.org/10.1029/2001JD900239, 2001.
- Brunner, D., Staehelin, J., Rogers, H. L., Köhler, M. O., Pyle, J. A., Hauglustaine, D. A., Jourdain, L., Berntsen, T. K., Gauss, M., Isaksen, I. S. A., Meijer, E., van Velthoven, P., Pitari, G., Mancini, E., Grewe, V., and Sausen, R.: An evaluation of the performance of chemistry transport models Part 2: Detailed comparison with two selected campaigns, Atmos. Chem. Phys., 5, 107–129, https://doi.org/10.5194/acp-5-107-2005, 2005.
- Bucsela, E. J., Perring, A. E., Cohen, R. C., Boersma, K. F., Celarier,
 E. A., Gleason, J. F., Wenig, M. O., Bertram, T. H., Wooldridge,
 P. J., Dirksen, R., and Veefkind, J. P.: Comparison of tropospheric
 NO₂ from in situ aircraft measurements with near-real-time and standard product data from OMI, J. Geophys. Res., 113, D16S31,
 https://doi.org/10.1029/2007JD008838, 2008.
- Carslaw, N., Carpenter, L. J., Plane, J. M. C., Allan, B. J., Burgess, R. A., Clemitshaw, K. C., Coe, H., and Penkett, S. A.: Simultaneous observations of nitrate and peroxy radicals in the marine boundary layer, J. Geophys. Res.-Atmos., 102, 18917–18933, https://doi.org/10.1029/97JD00399, 1997.
- Clough, P. N. and Thrush, B. A.: Mechanism of chemiluminescent reaction between nitric oxide and ozone, T. Faraday Soc., 63, 915–925, https://doi.org/10.1039/TF9676300915, 1967.
- Crawford, J., Davis, D., Chen, G., Bradshaw, J., Sandholm, S., Gregory, G., Sachse, G., Anderson, B., Collins, J., Blake, D., Singh, H., Heikes, B., Talbot, R., and Rodriguez, J.: Photostationary state analysis of the NO₂-NO system based on airborne observations from the western and central North Pacific, J. Geophys. Res.-Atmos., 101, 2053–2072, https://doi.org/10.1029/95JD02201, 1996.
- Creamean, J. M., Neiman, P. J., Coleman, T., Senff, C. J., Kirgis, G., Alvarez, R. J., and Yamamoto, A.: Colorado air quality impacted by long-range-transported aerosol: a set of case studies during the 2015 Pacific Northwest fires, Atmos. Chem. Phys., 16, 12329–12345, https://doi.org/10.5194/acp-16-12329-2016, 2016.
- Dee, D. P., Uppala, S. M., Simmons, A. J., Berrisford, P., Poli, P., Kobayashi, S., Andrae, U., Balmaseda, M. A., Balsamo, G., Bauer, P., Bechtold, P., Beljaars, A. C. M., van de Berg, L., Bidlot, J., Bormann, N., Delsol, C., Dragani, R., Fuentes, M., Geer, A. J., Haimberger, L., Healy, S. B., Hersbach, H., Hólm, E. V., Isaksen, L., Kållberg, P., Köhler, M., Matricardi, M., McNally, A. P., Monge-Sanz, B. M., Morcrette, J.-J., Park, B.-K., Peubey, C., de Rosnay, P., Tavolato, C., Thépaut, J.-N., and Vitart, F.: The ERA-Interim reanalysis: configuration and performance of the data assimilation system, Q. J. Roy. Meteorol. Soc., 137, 553–597, https://doi.org/10.1002/qj.828, 2011.
- de Laat, A. T. J., Aben, I., Deeter, M., Nédélec, P., Eskes, H., Attié, J.-L., Ricaud, P., Abida, R., El Amraoui, L., and Landgraf, J.: Validation of nine years of MOPITT V5 NIR using MOZAIC/IAGOS measurements: biases and long-term stability, Atmos. Meas. Tech., 7, 3783–3799, https://doi.org/10.5194/amt-7-3783-2014, 2014.

- Drummond, J. W., Volz, A., and Ehhalt, D. H.: An optimized chemiluminescence detector for tropospheric NO measurements, J. Atmos. Chem., 2, 287–306, https://doi.org/10.1007/BF00051078, 1985.
- Duncan, B. N., Lamsal, L. N., Thompson, A. M., Yoshida, Y., Lu, Z., Streets, D. G., Hurwitz, M. M., and Pickering, K. E.: A space-based, high-resolution view of notable changes in urban NO_x pollution around the world (2005–2014), J. Geophys. Res.-Atmos., 121, 976–996, https://doi.org/10.1002/2015JD024121, 2016.
- Ehhalt, D. H., Rohrer, F., and Wahner, a: Sources and Distribution of NO_x in the Upper Troposphere at Northern Mid-Latitudes, J. Geophys. Res.-Atmos., 97, 3725–3738, 1992.
- Emmons, L. K., Carroll, M. A., Hauglustaine, D. A., Brasseur, G. P., Atherton, C., Penner, J., Sillman, S., Levy, H., Rohrer, F., Wauben, W. M. F., Van Velthoven, P. F. J., Wang, Y., Jacob, D., Bakwin, P., Dickerson, R., Doddridge, B., Gerbig, C., Honrath, R., Hübler, G., Jaffe, D., Kondo, Y., Munger, J. W., Torres, A., and Volz-Thomas, A.: Climatologies of NO_{xx} and NO_y: A comparison of data and models, Atmos. Environ., 31, 1851–1904, https://doi.org/10.1016/S1352-2310(96)00334-2, 1997.
- Eskes, H. J. and Boersma, K. F.: Averaging kernels for DOAS total-column satellite retrievals, Atmos. Chem. Phys., 3, 1285–1291, https://doi.org/10.5194/acp-3-1285-2003, 2003.
- Fahey, D. W. and Lee, D. S.: Aviation and Climate Change?: A Scientific Perspective, Carbon Clim. Law Rev., 10,, 97–104, 2016.
- Fahey, D. W., Eubank, C. S., Hübler, G., and Fehsenfeld, F. C.: Evaluation of a catalytic reduction technique for the measurement of total reactive odd-nitrogen NO_y in the atmosphere, J. Atmos. Chem., 3, 435–468, https://doi.org/10.1007/bf00053871, 1985.
- Fehsenfeld, F. C., Drummond, J. W., Roychowdhury, U. K., Galvin, P. J., Williams, E. J., Burr, M. P., Parrish, D. D., Hobler, G., Langford, A. O., Calvert, J. G., Ridley, B. A., Heikes, B. G., Kok, G. L., Shetier, J. D., Walega, J. G., Elsworth, C. M., and Mohnen, V. A.: Intercomparison of NO₂ Measurement Techniques, J. Geophys. Res., 95, 3579–3597, https://doi.org/10.1029/JD095iD04p03579, 1990.
- Feigl, C.: Aufbau und Charakterisierung eines Meßsystems für NO, NO₂ und NO_y: Laboruntersuchungen und Einsatz in der unteren arktischen Stratosphäre, PhD thesis, Technische Universität, München, Germany, 1998.
- Fischer, E. V., Jacob, D. J., Yantosca, R. M., Sulprizio, M. P., Millet, D. B., Mao, J., Paulot, F., Singh, H. B., Roiger, A., Ries, L., Talbot, R. W., Dzepina, K., and Pandey Deolal, S.: Atmospheric peroxyacetyl nitrate (PAN): a global budget and source attribution, Atmos. Chem. Phys., 14, 2679–2698, https://doi.org/10.5194/acp-14-2679-2014, 2014.
- Fishman, J., Al-Saadi, J. A., Creilson, J. K., Bowman, K. W., Burrows, J. P., Richter, A., Chance, K. V., Edwards, D. P., Martin, R. V., Morris, G. A., Pierce, R. B., Ziemke, J. R., Schaack, T. K., and Thompson, A. M.: Remote Sensing of Tropospheric Pollution from Space, B. Am. Meteorol. Soc., 89, 805–821, https://doi.org/10.1175/2008BAMS2526.1, 2008.
- Fuchs, H., Ball, S. M., Bohn, B., Brauers, T., Cohen, R. C., Dorn,
 H.-P., Dubé, W. P., Fry, J. L., Häseler, R., Heitmann, U., Jones, R.
 L., Kleffmann, J., Mentel, T. F., Müsgen, P., Rohrer, F., Rollins,
 A. W., Ruth, A. A., Kiendler-Scharr, A., Schlosser, E., Shillings,
 A. J. L., Tillmann, R., Varma, R. M., Venables, D. S., Vil-

- lena Tapia, G., Wahner, A., Wegener, R., Wooldridge, P. J., and Brown, S. S.: Intercomparison of measurements of NO₂ concentrations in the atmosphere simulation chamber SAPHIR during the NO3Comp campaign, Atmos. Meas. Tech., 3, 21–37, https://doi.org/10.5194/amt-3-21-2010, 2010.
- Fueglistaler, S., Abalos, M., Flannaghan, T. J., Lin, P., and Randel, W. J.: Variability and trends in dynamical forcing of tropical lower stratospheric temperatures, Atmos. Chem. Phys., 14, 13439–13453, https://doi.org/10.5194/acp-14-13439-2014, 2014.
- Gerbig, C., Marshall, J., and IGAS Team: The IGAS project a bridge between IAGOS and the Copernicus Atmosphere Service, Geophys. Res. Abstr., 16, EGU2014-5849, available at: http://juser.fz-juelich.de/record/186699 (last access: 29 November 2017), 2014.
- Gressent, A., Sauvage, B., Defer, E., Pätz, H. W., Thomas, K., Holle, R., Cammas, J.-P., Nédélec, P., Boulanger, D., Thouret, V., and Volz-Thomas, A.: Lightning NO_x influence on large-scale NO_y and O_3 plumes observed over the northern mid-latitudes, Tellus B, 66, 25544, https://doi.org/10.3402/tellusb.v66.25544, 2014.
- Gressent, A., Sauvage, B., Cariolle, D., Evans, M., Leriche, M., Mari, C., and Thouret, V.: Modeling lightning-NO_x chemistry on a sub-grid scale in a global chemical transport model, Atmos. Chem. Phys., 16, 5867–5889, https://doi.org/10.5194/acp-16-5867-2016, 2016.
- Huntrieser, H., Lichtenstern, M., Scheibe, M., Aufmhoff, H.,
 Schlager, H., Pucik, T., Minikin, A., Weinzierl, B., Heimerl,
 K., Pollack, I. B., Peischl, J., Ryerson, T. B., Weinheimer, A.
 J., Honomichl, S., Ridley, B. A., Biggerstaff, M. I., Betten, D.
 P., Hair, J. W., Butler, C. F., Schwartz, M. J., and Barth, M.
 C.: Injection of lightning-produced NO_x, water vapor, wildfire emissions, and stratospheric air to the UT/LS as observed from
 DC3 measurements, J. Geophys. Res.-Atmos., 121, 6638–6668,
 https://doi.org/10.1002/2015JD024273, 2016.
- IPCC: Climate Change 2007: The Physical Science Basis. Contribution of Working Group I to the Fourth Assessment Report of the Intergovernmental Panel on Climate Change, edited by: Solomon, S., Qin, D., Manning, M., Z. Chen, Z., Marquis, M., Averyt, K. B., Tignor, M., and Miller, H. L., Cambridge University Press, UK and New York, USA, 2007.
- Jurkat, T., Voigt, C., Arnold, F., Schlager, H., Kleffmann, J., Aufmhoff, H., Schuble, D., Schaefer, M., and Schumann, U.: Measurements of HONO, NO, NO_y and SO₂ in aircraft exhaust plumes at cruise, Geophys. Res. Lett., 38, 1–5, https://doi.org/10.1029/2011GL046884, 2011.
- Jurkat, T., Kaufmann, S., Voigt, C., Schäuble, D., Jeßberger, P., and Ziereis, H.: The airborne mass spectrometer AIMS – Part 2: Measurements of trace gases with stratospheric or tropospheric origin in the UTLS, Atmos. Meas. Tech., 9, 1907–1923, https://doi.org/10.5194/amt-9-1907-2016, 2016.
- Kebabian, P. L., Wood, E. C., Herndon, S. C., and Freedman, A.: A practical alternative to chemiluminescence-based detection of nitrogen dioxide: Cavity attenuated phase shift spectroscopy, Environ. Sci. Technol., 42, 6040–6045, https://doi.org/10.1021/es703204j, 2008.
- Kim, S., Huey, L. G., Stickel, R. E., Tanner, D. J., Crawford, J. H., Olson, J. R., Chen, G., Brune, W. H., Ren, X., Lesher, R., Wooldridge, P. J., Bertram, T. H., Perring,

- A., Cohen, R. C., Lefer, B. L., Shetter, R. E., Avery, M., Diskin, G., and Sokolik, I.: Measurement of HO₂NO₂ in the free troposphere during the Intercontinental Chemical Transport Experiment–North America 2004, J. Geophys. Res., 112, D12S01, https://doi.org/10.1029/2006JD007676, 2007.
- Kunz, A., Pan, L. L., Konopka, P., Kinnison, D. E., and Tilmes, S.: Chemical and dynamical discontinuity at the extratropical tropopause based on START08 and WACCM analyses, J. Geophys. Res.-Atmos., 116, 1–15, https://doi.org/10.1029/2011JD016686, 2011.
- Laughner, J. L., Zare, A., and Cohen, R. C.: Effects of daily meteorology on the interpretation of space-based remote sensing of NO₂, Atmos. Chem. Phys., 16, 15247–15264, https://doi.org/10.5194/acp-16-15247-2016, 2016.
- Lee, D. S., Pitari, G., Grewe, V., Gierens, K., Penner, J. E., Petzold, A., Prather, M. J., Schumann, U., Bais, A., and Berntsen, T.: Transport impacts on atmosphere and climate: Aviation, Atmos. Environ., 44, 4678–4734, https://doi.org/10.1016/j.atmosenv.2009.06.005, 2010.
- Lindaas, J., Farmer, D. K., Pollack, I. B., Abeleira, A., Flocke, F., Roscioli, R., Herndon, S., and Fischer, E. V.: Changes in ozone and precursors during two aged wildfire smoke events in the Colorado Front Range in summer 2015, Atmos. Chem. Phys., 17, 10691–10707, https://doi.org/10.5194/acp-17-10691-2017, 2017.
- Marenco, A., Thouret, V., Nédélec, P., Smit, H., Helten, M., Kley, D., Karcher, F., Simon, P., Law, K., Pyle, J., Poschmann, G., Von Wrede, R., Hume, C., and Cook, T.: Measurement of ozone and water vapor by Airbus in-service aircraft: The MOZAIC airborne program, an overview, J. Geophys. Res.-Atmos., 103, 25631–25642, https://doi.org/10.1029/98JD00977, 1998.
- Monks, P. S., Granier, C., Fuzzi, S., Stohl, A., Williams, M. L., Akimoto, H., Amann, M., Baklanov, A., Baltensperger, U., Bey, I., Blake, N., Blake, R. S., Carslaw, K., Cooper, O. R., Dentener, F., Fowler, D., Fragkou, E., Frost, G. J., Generoso, S., Ginoux, P., Grewe, V., Guenther, A., Hansson, H. C., Henne, S., Hjorth, J., Hofzumahaus, A., Huntrieser, H., Isaksen, I. S. A., Jenkin, M. E., Kaiser, J., Kanakidou, M., Klimont, Z., Kulmala, M., Laj, P., Lawrence, M. G., Lee, J. D., Liousse, C., Maione, M., McFiggans, G., Metzger, A., Mieville, A., Moussiopoulos, N., Orlando, J. J., O'Dowd, C. D., Palmer, P. I., Parrish, D. D., Petzold, A., Platt, U., Pöschl, U., Prévôt, A. S. H., Reeves, C. E., Reimann, S., Rudich, Y., Sellegri, K., Steinbrecher, R., Simpson, D., ten Brink, H., Theloke, J., van der Werf, G. R., Vautard, R., Vestreng, V., Vlachokostas, C., and von Glasow, R.: Atmospheric composition change - global and regional air quality, Atmos. Environ., 43, 5268–5350, https://doi.org/10.1016/j.atmosenv.2009.08.021,
- Moore, D. P. and Remedios, J. J.: Seasonality of Peroxyacetyl nitrate (PAN) in the upper troposphere and lower stratosphere using the MIPAS-E instrument, Atmos. Chem. Phys., 10, 6117–6128, https://doi.org/10.5194/acp-10-6117-2010, 2010.
- Nakamura, K., Kondo, Y., Chen, G., Crawford, J. H., Takegawa, N., Koike, M., Kita, K., Miyazaki, Y., Shetter, R. E., Lefer, B. L., Avery, M., and Matsumoto, J.: Measurement of NO₂ by the photolysis conversion technique during the Transport and Chemical Evolution Over the Pacific (TRACE-P) campaign, J. Geophys. Res.-Atmos., 108, 4752, https://doi.org/10.1029/2003JD003712, 2003

- Nédélec, P., Blot, R., Boulanger, D., Athier, G., Cousin, J.-M., Gautron, B., Petzold, A., Volz-Thomas, A., and Thouret, V.: Instrumentation on commercial aircraft for monitoring the atmospheric composition on a global scale: the IAGOS system, technical overview of ozone and carbon monoxide measurements, Tellus B, 67, 1–16, https://doi.org/10.3402/tellusb.v67.27791, 2015.
- Neis, P., Smit, H. G. J., Rohs, S., Bundke, U., Krämer, M., Spelten, N., Ebert, V., Buchholz, B., Thomas, K., and Petzold, A.: Quality assessment of MOZAIC and IAGOS capacitive hygrometers: insights from airborne field studies, Tellus B, 67, 28320, https://doi.org/10.3402/tellusb.v67.28320, 2015.
- Parrish, D. D., Hahn, C. H., Fahey, D. W., Williams, E. J., Bollinger, M. J., Hübler, G., Buhr, M. P., Murphy, P. C., Trainer, M., Hsie, E. Y., Liu, S. C., and Fehsenfeld, F. C.: Systematic variations in the concentration of NO_x (NO Plus NO₂) at Niwot Ridge, Colorado, J. Geophys. Res., 95, 1817, https://doi.org/10.1029/JD095iD02p01817, 1990.
- Pätz, H.-W., Lerner, A., Houben, N., and Volz-Thomas, A.: Validierung eines neuen Verfahrens zur Kalibrierung von Peroxiacetylnitrat (PAN)-Analysatoren, Gefahrstoffe. Reinhaltung der Luft. Air Quality Control, 62, 215–220, 2002.
- Pätz, H.-W., Volz-Thomas, A., Hegglin, M. I., Brunner, D., Fischer, H., and Schmidt, U.: In-situ comparison of the NO_y instruments flown in MOZAIC and SPURT, Atmos. Chem. Phys., 6, 2401–2410, https://doi.org/10.5194/acp-6-2401-2006, 2006.
- Petzold, A., Thouret, V., Gerbig, C., Zahn, A., Brenninkmeijer, C. A. M., Gallagher, M., Hermann, M., Pontaud, M., Ziereis, H., Boulanger, D., Marshall, J., Nédélec, P., Smit, H. G. J., Friess, U., Flaud, J.-M., Wahner, A., Cammas, J.-P., and Volz-Thomas, A.: Global-scale atmosphere monitoring by in-service aircraft current achievements and future prospects of the European Research Infrastructure IAGOS, Tellus B, 67, 1–24, https://doi.org/10.3402/tellusb.v67.28452, 2015.
- Piters, A. J. M., Boersma, K. F., Kroon, M., Hains, J. C., Van Roozendael, M., Wittrock, F., Abuhassan, N., Adams, C., Akrami, M., Allaart, M. A. F., Apituley, A., Beirle, S., Bergwerff, J. B., Berkhout, A. J. C., Brunner, D., Cede, A., Chong, J., Clémer, K., Fayt, C., Frieß, U., Gast, L. F. L., Gil-Ojeda, M., Goutail, F., Graves, R., Griesfeller, A., Großmann, K., Hemerijckx, G., Hendrick, F., Henzing, B., Herman, J., Hermans, C., Hoexum, M., van der Hoff, G. R., Irie, H., Johnston, P. V., Kanaya, Y., Kim, Y. J., Klein Baltink, H., Kreher, K., de Leeuw, G., Leigh, R., Merlaud, A., Moerman, M. M., Monks, P. S., Mount, G. H., Navarro-Comas, M., Oetjen, H., Pazmino, A., Perez-Camacho, M., Peters, E., du Piesanie, A., Pinardi, G., Puentedura, O., Richter, A., Roscoe, H. K., Schönhardt, A., Schwarzenbach, B., Shaiganfar, R., Sluis, W., Spinei, E., Stolk, A. P., Strong, K., Swart, D. P. J., Takashima, H., Vlemmix, T., Vrekoussis, M., Wagner, T., Whyte, C., Wilson, K. M., Yela, M., Yilmaz, S., Zieger, P., and Zhou, Y.: The Cabauw Intercomparison campaign for Nitrogen Dioxide measuring Instruments (CINDI): design, execution, and early results, Atmos. Meas. Tech., 5, 457-485, https://doi.org/10.5194/amt-5-457-2012, 2012.
- Platt, U. and Stutz, J.: Differential optical absorption spectroscopy, Physics of Earth and Space Environments, Springer Berlin Heidelberg, Germany, https://doi.org/10.1007/978-3-540-75776-4, 2008.

- Pollack, I. B., Lerner, B. M., and Ryerson, T. B.: Evaluation of ultraviolet light-emitting diodes for detection of atmospheric NO₂ by photolysis Chemiluminescence, J. Atmos. Chem., 65, 111–125, https://doi.org/10.1007/s10874-011-9184-3, 2010.
- Pollack, I. B., Ryerson, T. B., Trainer, M., Parrish, D. D., Andrews, A. E., Atlas, E. L., Blake, D. R., Brown, S. S., Commane, R., Daube, B. C., De Gouw, J. A., Dubé, W. P., Flynn, J., Frost, G. J., Gilman, J. B., Grossberg, N., Holloway, J. S., Kofler, J., Kort, E. A., Kuster, W. C., Lang, P. M., Lefer, B., Lueb, R. A., Neuman, J. A., Nowak, J. B., Novelli, P. C., Peischl, J., Perring, A. E., Roberts, J. M., Santoni, G., Schwarz, J. P., Spackman, J. R., Wagner, N. L., Warneke, C., Washenfelder, R. A., Wofsy, S. C., and Xiang, B.: Airborne and ground-based observations of a weekend effect in ozone, precursors, and oxidation products in the California South Coast Air Basin, J. Geophys. Res.-Atmos., 117, 1–14, https://doi.org/10.1029/2011JD016772, 2012.
- Prather, M. J., Zhu, X., Flynn, C. M., Strode, S. A., Rodriguez, J. M., Steenrod, S. D., Liu, J., Lamarque, J.-F., Fiore, A. M., Horowitz, L. W., Mao, J., Murray, L. T., Shindell, D. T., and Wofsy, S. C.: Global atmospheric chemistry which air matters, Atmos. Chem. Phys., 17, 9081–9102, https://doi.org/10.5194/acp-17-9081-2017, 2017.
- Reed, C., Evans, M. J., Di Carlo, P., Lee, J. D., and Carpenter, L. J.: Interferences in photolytic NO₂ measurements: explanation for an apparent missing oxidant?, Atmos. Chem. Phys., 16, 4707– 4724, https://doi.org/10.5194/acp-16-4707-2016, 2016.
- Ridley, B. A. and Howlett, L. C.: An instrument for nitric oxide measurements in the stratosphere, Rev. Sci. Instrum., 45, 742–746, https://doi.org/10.1063/1.1686726, 1974.
- Ridley, B. A., Grahek, F. E., and Walega, J. G.: A Small High-Sensitivity, Medium-Response Ozone Detector Suitable for Measurements from Light Aircraft, J. Atmos. Ocean. Tech., 9, 142–148, https://doi.org/10.1175/1520-0426(1992)009<0142:ASHSMR>2.0.CO;2, 1992.
- Rohrer, F., Brüning, D., and Ehhalt, D. H.: Tropospheric mixing ratios of NO obtained during TROPOZ II in the latitude region 67° N–56° S, J. Geophys. Res.-Atmos., 102, 25429–25449, https://doi.org/10.1029/97JD01853, 1997.
- Ryerson, T. B., Williams, E. J., and Fehsenfeld, F. C.: An efficient photolysis system for fast response NO₂ measurements, J. Geophys. Res., 105, 26447–26461, https://doi.org/10.1029/2000JD900389, 2000.
- Schumann, U. and Huntrieser, H.: The global lightning-induced nitrogen oxides source, Atmos. Chem. Phys., 7, 3823–3907, https://doi.org/10.5194/acp-7-3823-2007, 2007.
- Skalska, K., Miller, J. S., and Ledakowicz, S.: Trends in NO_x abatement: A review, Sci. Total Environ., 408, 3976–3989, https://doi.org/10.1016/j.scitotenv.2010.06.001, 2010.
- Sprung, D. and Zahn, A.: Acetone in the upper troposphere/lowermost stratosphere measured by the CARIBIC passenger aircraft: Distribution, seasonal cycle, and variability, J. Geophys. Res.-Atmos., 115, 1–12, https://doi.org/10.1029/2009JD012099, 2010.
- Stohl, A., Forster, C., Frank, A., Seibert, P., and Wotawa, G.: Technical note: The Lagrangian particle dispersion model FLEXPART version 6.2, Atmos. Chem. Phys., 5, 2461–2474, https://doi.org/10.5194/acp-5-2461-2005, 2005.
- Stratmann, G., Ziereis, H., Stock, P., Brenninkmeijer, C. A. M., Zahn, A., Rauthe-Schöch, A., Velthoven, P. V., Schlager,

- H., and Volz-Thomas, A.: NO and NO_y in the upper troposphere: Nine years of CARIBIC measurements on-board a passenger aircraft, Atmos. Environ., 133, 93–111, https://doi.org/10.1016/j.atmosenv.2016.02.035, 2016.
- Thomas, K., Berg, M., Boulanger, D., Houben, N., Gressent, A., Nédélec, P., Pätz, H.-W., Thouret, V., and Volz-Thomas, A.: Climatology of NO_y in the troposphere and UT/LS from measurements made in MOZAIC, Tellus B, 67, 1–16, https://doi.org/10.3402/tellusb.v67.28793, 2015.
- Thornton, J. A., Wooldridge, P. J., and Cohen, R. C.: Atmospheric NO₂?: In Situ Laser-Induced Fluorescence Detection at Parts per Trillion Mixing Ratios, Anal. Chem., 72, 528–539, https://doi.org/10.1021/ac9908905, 2000.
- Thouret, V., Cammas, J.-P., Sauvage, B., Athier, G., Zbinden, R., Nédélec, P., Simon, P., and Karcher, F.: Tropopause referenced ozone climatology and inter-annual variability (1994–2003) from the MOZAIC programme, Atmos. Chem. Phys., 6, 1033–1051, https://doi.org/10.5194/acp-6-1033-2006, 2006.
- Veefkind, J. P., Aben, I., McMullan, K., Förster, H., de Vries, J., Otter, G., Claas, J., Eskes, H. J., de Haan, J. F., Kleipool, Q., van Weele, M., Hasekamp, O., Hoogeveen, R., Landgraf, J., Snel, R., Tol, P., Ingmann, P., Voors, R., Kruizinga, B., Vink, R., Visser, H., and Levelt, P. F.: TROPOMI on the ESA Sentinel-5 Precursor: A GMES mission for global observations of the atmospheric composition for climate, air quality and ozone layer applications, Remote Sens. Environ., 120, 70–83, https://doi.org/10.1016/j.rse.2011.09.027, 2012.
- Villena, G., Bejan, I., Kurtenbach, R., Wiesen, P., and Kleffmann, J.: Interferences of commercial NO₂ instruments in the urban atmosphere and in a smog chamber, Atmos. Meas. Tech., 5, 149–159, https://doi.org/10.5194/amt-5-149-2012, 2012.
- Volz-Thomas, A., Xueref, I., and Schmitt, R.: An automatic gas chromatograph and calibration system for ambient measurements of PAN and PPN, Environ. Sci. Pollut. R., 9, 72–76, 2002.
- Volz-Thomas, A., Berg, M., Heil, T., Houben, N., Lerner, A., Petrick, W., Raak, D., and Pätz, H.-W.: Measurements of total odd nitrogen (NO_y) aboard MOZAIC in-service aircraft: instrument design, operation and performance, Atmos. Chem. Phys., 5, 583–595, https://doi.org/10.5194/acp-5-583-2005, 2005.

- Wagner, N. L., Dubé, W. P., Washenfelder, R. A., Young, C. J., Pollack, I. B., Ryerson, T. B., and Brown, S. S.: Diode laser-based cavity ring-down instrument for NO₃, N₂O₅, NO, NO₂ and O₃ from aircraft, Atmos. Meas. Tech., 4, 1227–1240, https://doi.org/10.5194/amt-4-1227-2011, 2011.
- Wasiuk, D. K., Khan, M. A. H., Shallcross, D. E., Derwent, R. G., and Lowenberg, M. H.: A mitigation strategy for commercial aviation impact on NO_x-related O₃ change, J. Geophys. Res.-Atmos., 121, 8730–8740, https://doi.org/10.1002/2016JD025051, 2016.
- Yang, J., Honrath, R. E., Peterson, M. C., Parrish, D. D., and Warshawsky, M.: Photostationary state deviation-estimated peroxy radicals and their implications for HO_x and ozone photochemistry at a remote northern Atlantic coastal site, J. Geophys. Res., 109, D02312, https://doi.org/10.1029/2003jd003983, 2004.
- Zbinden, R. M., Thouret, V., Ricaud, P., Carminati, F., Cammas, J.-P., and Nédélec, P.: Climatology of pure tropospheric profiles and column contents of ozone and carbon monoxide using MOZAIC in the mid-northern latitudes (24° N to 50° N) from 1994 to 2009, Atmos. Chem. Phys., 13, 12363–12388, https://doi.org/10.5194/acp-13-12363-2013, 2013.
- Ziereis, H., Schlager, H., Schulte, P., Köhler, I., Marquardt, R., and Feigl, C.: In situ measurements of the NO_x distribution and variability over the eastern North Atlantic, J. Geophys. Res.-Atmos., 104, 16021–16032, https://doi.org/10.1029/1999JD900175, 1999.
- Ziereis, H., Schlager, H., and Schulte, P.: Distributions of NO, NO_x, and NO_y in the upper troposphere and lower stratosphere between 28 and 61° N during POLINAT, J. Geophys. Res., 105, 3653–3664, 2000.